cmgh
CELLULAR AND MOLECULAR GASTROENTEROLOGY AND HEPATOLOGY

ORIGINAL RESEARCH

USP25 Deficiency Exacerbates Acute Pancreatitis via Up-Regulating TBK1–NF-κB Signaling in Macrophages

Xin Liu,[1] Wu Luo,[2] Jiahao Chen,[1] Chenghong Hu,[1] Rumbidzai N. Mutsinze,[1] Xu Wang,[1] Yanmei Zhang,[3] Lijiang Huang,[4] Wei Zuo,[4] Guang Liang,[1,3] and Yi Wang[1,4]

[1]Chemical Biology Research Center, School of Pharmaceutical Sciences, Wenzhou Medical University, Wenzhou, Zhejiang, China; [2]Medical Research Center, First Affiliated Hospital, Wenzhou Medical University, Wenzhou, Zhejiang, China; [3]School of Pharmaceutical Sciences, Hangzhou Medical College, Hangzhou, Zhejiang, China; and [4]Department of Gastroenterology, Affiliated Xiangshan Hospital of Wenzhou Medial University, Xiangshan, Zhejiang, China

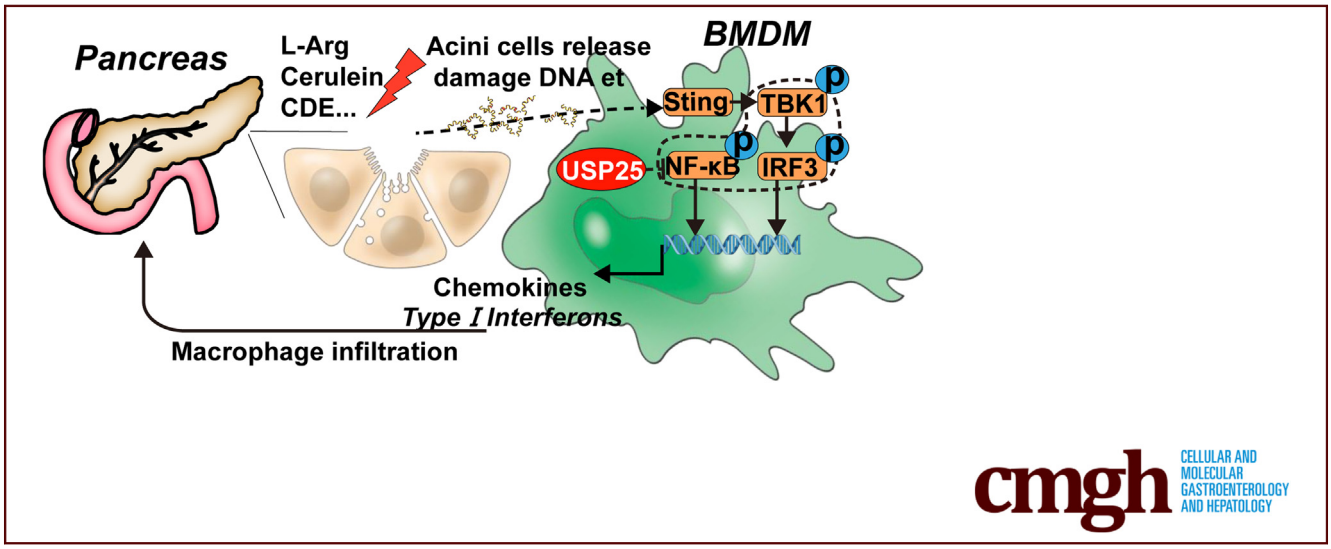

SUMMARY

Deficiency of macrophage ubiquitin-specific protease 25 enhances the activation of the TANK-binding kinase 1/nuclear factor-κB pathway, causing pancreatic and lung injury in different acute pancreatitis mouse models. Approaches to increase ubiquitin-specific protease 25 expression and function in macrophages may provide an anti-inflammatory therapy for acute pancreatitis.

BACKGROUND & AIMS: Severe acute pancreatitis can easily lead to systemic inflammatory response syndrome and death. Macrophages are known to be involved in the pathophysiology of acute pancreatitis (AP), and macrophage activation correlates with disease severity. In this study, we examined the role of ubiquitin-specific protease 25, a deubiquitinating enzyme and known regulator of macrophages, in the pathogenesis of AP.

METHODS: We used L-arginine, cerulein, and choline-deficient ethionine-supplemented diet–induced models of AP in *Usp25*$^{-/-}$ mice and wild-type mice. We also generated bone marrow *Usp25*$^{-/-}$ chimeric mice and initiated L-arginine–mediated AP. Primary acinar cells and bone marrow–derived macrophages were isolated from wild-type and *Usp25*$^{-/-}$ mice to dissect molecular mechanisms.

RESULTS: Our results show that *Usp25* deficiency exacerbates pancreatic and lung injury, neutrophil and macrophage infiltration, and systemic inflammatory responses in L-arginine, cerulein, and choline-deficient ethionine-supplemented diet–induced models of AP. Bone marrow *Usp25*$^{-/-}$ chimeric mice challenged with L-arginine show that *Usp25* deficiency in macrophages exaggerates AP by up-regulating the TANK-binding kinase 1 (TBK1)–nuclear factor-κB (NF-κB) signaling pathway. Similarly, in vitro data confirm that *Usp25* deficiency enhances the TBK1–NF-κB pathway, leading to increased expression of inflammatory cytokines in bone marrow–derived macrophages.

CONCLUSIONS: *Usp25* deficiency in macrophages enhances TBK1–NF-κB signaling, and the induction of inflammatory chemokines and type I interferon-related genes exacerbates pancreatic and lung injury in AP. *(Cell Mol Gastroenterol Hepatol 2022;14:1103–1122; https://doi.org/10.1016/j.jcmgh.2022.07.013)*

Keywords: Severe Acute Pancreatitis; Deubiquitinating Enzymes; Systemic Inflammatory Response Syndrome; Bone Marrow–Derived Macrophages.

Acute pancreatitis (AP) is a digestive system disease that comes on suddenly and requires hospitalization.[1] Obstruction by gallstones is a common cause of AP.[2] Alcohol consumption and smoking also can increase the

risk of AP.[3,4] Clinically, most patients present with mild AP, which usually is self-limiting, and patients recover quickly. However, approximately 20% of the patients progress to severe AP, which carries a high mortality rate and requires intensive treatment.[5–7] Severe AP easily can lead to systemic inflammatory response syndrome and multiple organ dysfunction syndrome. Among the complications associated with severe AP, acute lung injury is one of the most serious diseases.[5,8,9] Unfortunately, the pathogenesis of severe AP-associated multiple organ dysfunction syndrome is not fully understood, but may involve pancreatic necrosis, bacteremia, intestinal barrier failure, and activation of inflammatory cascades and diffuse alveolar damage.[10–13]

Clinical studies have shown that several inflammatory cytokines predict and mark AP disease severity.[14] Corroborating experimental studies have highlighted the critical role of innate immune activation, neutrophils, and macrophages in AP.[15–17] These studies suggest that mechanisms suppressing inflammatory responses should be explored for AP. In this context, the ubiquitin-specific protease 25 (USP25) warrants investigation.[18] USP25 is a deubiquitinating enzyme that prevents proteasomal degradation of substrates by hydrolyzing ubiquitin moieties conjugated to substrates. USP25 has been associated with antiviral immunity, Alzheimer's disease, cancers, diabetes, and other metabolic diseases.[19] Specifically, expression of USP25 decreases lipopolysaccharide-induced inflammatory cytokine production in macrophages, and negatively regulates virus-induced type I interferon signaling in Human embryonic kidney (HEK)-293T cells.[20,21,22] Based on this important role of USP25 in the suppression of inflammatory responses, we explored whether USP25 is involved in AP pathogenesis.

To investigate the role of USP25 in AP, AP was induced in *Usp25* knockout (KO) mice through L-arginine, cerulein, or choline-deficient diet supplemented with dextroisomer and Levoisomer-ethionine (CDE). Compared with wild-type (WT) mice, *Usp25* KO mice show aggravated AP, associated with increased inflammatory responses in the pancreas and lungs. Furthermore, USP25 expression in macrophages was shown to play a vital role in L-arginine–induced severe AP using a bone marrow transplantation chimeric mouse model. In vitro studies showed that *Usp25*$^{-/-}$ macrophages increase cytokine release after incubation with acinar cell supernatant (ACS) through activating the TANK-binding kinase 1 (TBK1) and nuclear factor-κB (NF-κB) signaling pathways. Our studies have shown a novel role of USP25 in AP pathogenesis.

Results

Usp25$^{-/-}$ Mice Show Aggravated L-Arginine–Induced Severe AP and Associated Lung Injury

We first used the L-arginine model of severe AP.[23] WT and *Usp25*$^{-/-}$ mice received 2 × 4 g/kg L-arginine and were killed 72 hours after the first injection, the point of peak pancreatic injury. Gross morphology of the harvested pancreas (Figure 1*A*) and pancreas-to-body weight ratios (Figure 1*B*) indicated edema after L-arginine injections, which was more severe in the *Usp25*$^{-/-}$ mice compared with WT mice. Pancreas injury was evaluated further by measuring the levels of serum amylase, lactate dehydrogenase (LDH), and lipase. These biochemical parameters were increased significantly after L-arginine administration (Figure 1*B*). Furthermore, the increase was greater in *Usp25*$^{-/-}$ mice compared with WT mice. Histopathologic assessment of pancreas showed increased pancreatic edema, inflammatory infiltration, and necrosis in *Usp25*$^{-/-}$ mice challenged with L-arginine compared with WT mice (Figure 1*C* and 1*D*).

We next examined lung tissues in mice challenged with L-arginine because acute lung injury is one of the common complications of severe AP. Compared with the WT mice, the *Usp25*$^{-/-}$ mice showed severe structural alterations as evident through histopathologic analysis (Figure 2*A*). Staining of lung tissues showed increased macrophage F4/80 antigen immunoreactivity in *Usp25*$^{-/-}$ mice compared with WT mice (Figure 2*B* and *C*). Furthermore, myeloperoxidase (MPO) activity was significantly higher in L-arginine–challenged mice, and in *Usp25*$^{-/-}$ compared with WT mice (Figure 2*E*). Increased F4/80 immunoreactivity and MPO activity followed the same pattern in pancreas (Figure 2*B*, *D*, *F*). In line with these results, pancreatitis-induced trypsinogen activation in the pancreas was significantly higher in *Usp25*$^{-/-}$ mice compared with WT mice (Figure 2*G*). These results indicated that *Usp25* deficiency aggravates pancreatic injury and inflammatory cell infiltration in the L-arginine–induced model of severe AP.

Usp25 Deletion in Bone Marrow–Derived Macrophages Aggravates L-Arginine–Induced Severe AP

Based on our observation of increased macrophage F4/80 immunoreactivity in the pancreas and lung tissues of *Usp25*$^{-/-}$ mice challenged with L-arginine, as well as the known critical role of macrophages in AP,[24] we explored the contribution of macrophage USP25 in AP. WT mice were irradiated and reconstituted with bone marrow cells derived from either WT donor mice or *Usp25*$^{-/-}$ mice. Similar to *Usp25*$^{-/-}$ mice challenged with L-arginine, WT mice, after receiving *Usp25*$^{-/-}$ bone marrow cells (KO→WT), showed severe pancreatic injury compared with WT mice that received WT bone marrow cells (WT→WT). This was

Abbreviations used in this paper: **ACS, acinar cell supernatant; AP, acute pancreatitis; BMDM, bone marrow–derived macrophage; BSA, bovine serum albumin; CD, chow diet; CDE, choline-deficient ethionine-supplemented diet; DMEM, Dulbecco's modified Eagle medium; DMXAA, Dimethylxanthine acetic acid; ELISA, enzyme-linked immunosorbent assay; IFN, interferon; IL, interleukin; IRF3, phosphorylated interferon regulatory factor 3; JNK, c-Jun-N-terminal kinase; KO, knockout; LDH, lactate dehydrogenase; MPO, myeloperoxidase; NF-κB, nuclear factor-κB; SBTI, soybean trypsin inhibitor; P65, P65 protein; STING, stimulator of interferon genes; TBK1, TANK-binding kinase 1; TLR, Toll-like receptor; TRAF, tumor necrosis factor receptor–associated factor; USP25, ubiquitin-specific protease 25; WT, wild-type.**

Most current article

2352-345X
https://doi.org/10.1016/j.jcmgh.2022.07.013

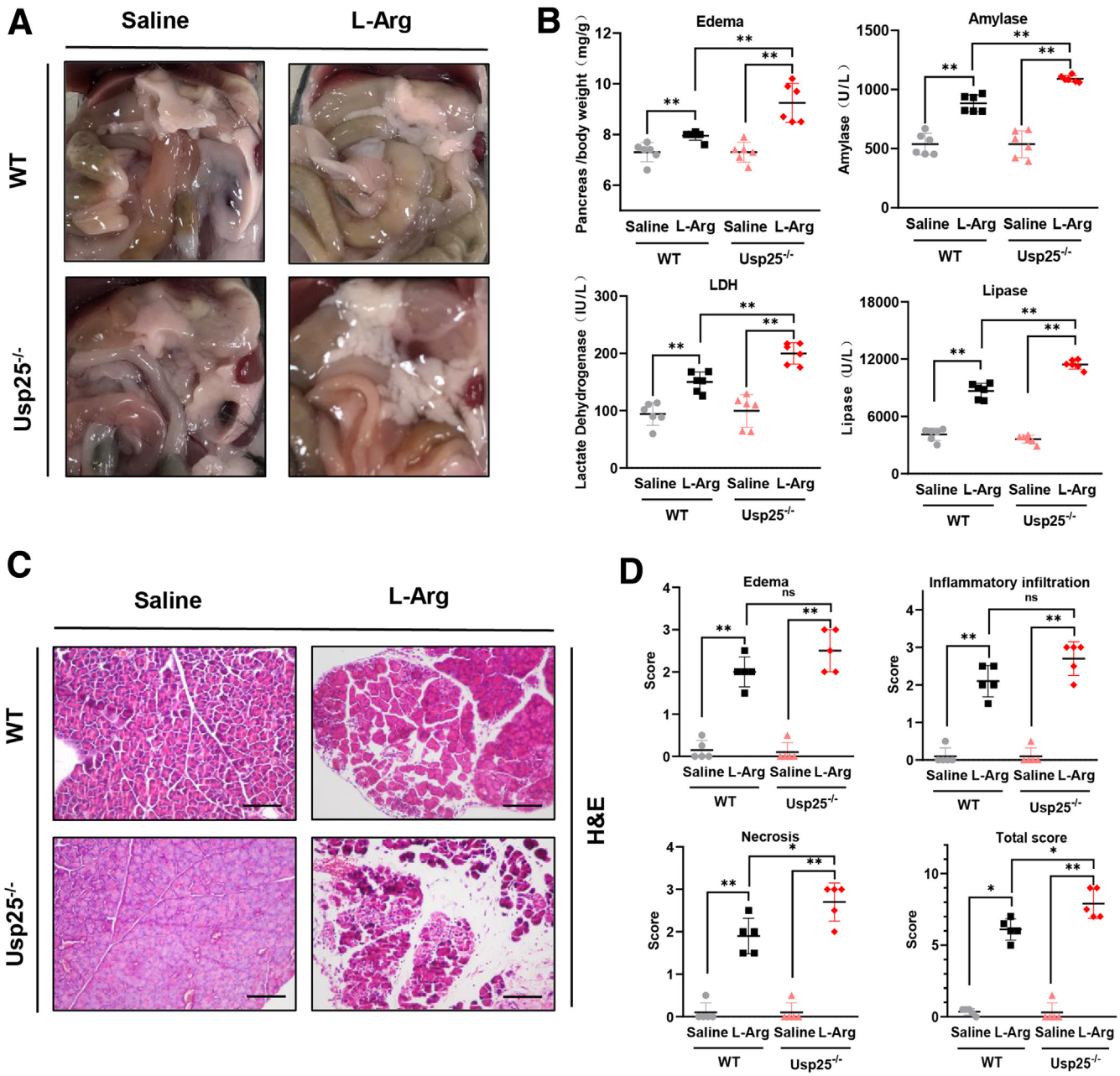

Figure 1. *Usp25* knockout mice show exacerbated L-arginine–induced pancreatitis. (*A*) Gross morphology of the pancreas 72 hours after injection of saline or L-arginine (L-Arg) in WT and *Usp25*$^{-/-}$ mice. (*B*) Pancreas-to-body-weight ratios, and serum levels of amylase, LDH, and lipase in mice. (*C*) Representative images of H&E-stained pancreatic tissues from mice. *Scale bar*: 100 μm. (*D*) Histopathologic scoring of pancreas tissues. (*B* and *D*) Data shown are means ± SD; n = 5–6. *$P < .05$ and **$P < .01$.

evident in gross tissue examination (Figure 3*A*), and pancreatic-to-body weight ratios, and levels of serum amylase, LDH, and lipase (Figure 3*B*). Histopathology confirmed that KO→WT mice had higher injury scores of edema, inflammatory infiltration, and necrosis (Figure 3*C* and *D*). Furthermore, F4/80 immunoreactivity in pancreas and lung (Figure 3*E*–*G*), MPO activity (Figure 3*H* and *I*), and pancreatic trypsin activity (Figure 3*J*) all were higher in KO→WT mice compared with WT→WT mice. These data indicate that USP25 expression in macrophages plays a critical role in L-arginine–induced severe AP.

TBK1–NF-κB Activation in Macrophages by Acinar-Derived Factors Requires USP25 Expression

To further explore the role of macrophage USP25 in AP, we exposed bone marrow–derived macrophages (BMDMs) from WT and *Usp25*$^{-/-}$ mice to supernatants prepared from primary acinar cells (Figure 4*A*). Trypan blue staining showed that primary acinar preparation is viable (data not shown). Based on this observation, we collected ACS from WT cells only at 0 hours (immediately after culture) and 24

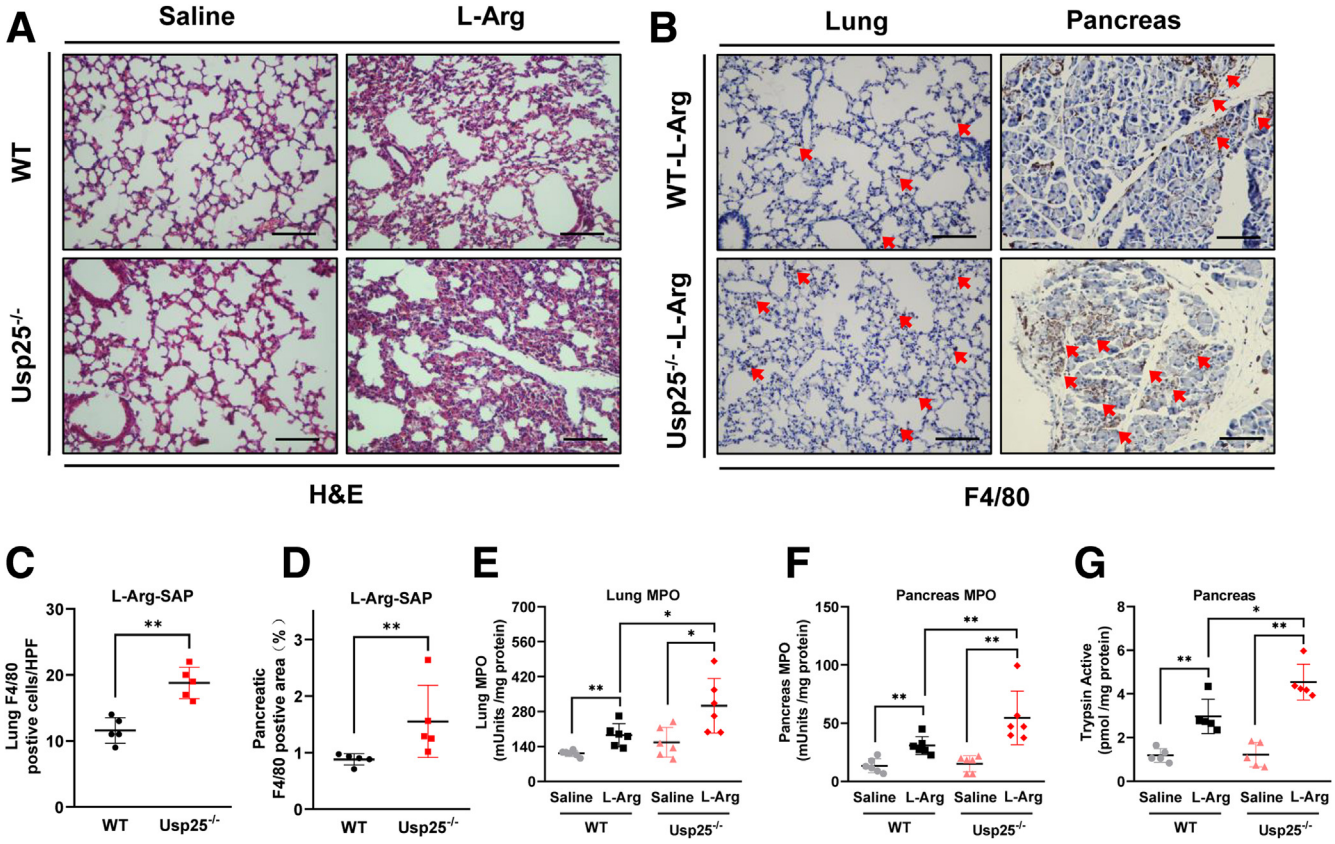

Figure 2. Increased inflammatory cell infiltration in *Usp25*-deficient mice after L-arginine (L-Arg) administration. (*A*) Representative images of H&E-stained sections of lungs. *Scale bar*: 100 μm. (*B*) Representative immunohistochemical staining of lung and pancreas for macrophage F4/80 antigen. *Red arrows* indicate positive staining. *Scale bar*: 100 μm. Quantification of F4/80-immunoreactive (staining positive) area per high-power field (HPF) in (*C*) lung and (*D*) pancreatic tissues of mice. MPO activity in (*E*) lung and (*F*) pancreas of experimental mice. (*G*) Trypsin activity in the pancreas of mice. (*E*–*G*) Data shown are means ± SD; n = 5–6. **P* < .05, and ***P* < .01. SAP, severe acute pancreatitis.

hours. Supernatant then was applied to BMDMs to examine downstream activation.

A recent study showed that stimulator of interferon (IFN) genes (STING) and TBK1/NF-κB pathways promote inflammation in experimental AP.[12] This prompted us to examine whether acinar-derived factors alter STING/TBK1/NF-κB in macrophages derived from WT and *Usp25*$^{-/-}$ mice. Phosphorylated forms of TBK1, phosphorylated interferon regulatory factor 3 (IRF3), and P65 protein (P65), as well as the total STING protein levels, were induced in WT BMDMs that were exposed to ACS for 24 hours (Figure 4*B*). Interestingly, we found that these changes were exaggerated significantly in BMDMs harvested from *Usp25*$^{-/-}$, except for STING protein levels, which did not appear to increase (Figure 4*B*). Transcript levels of inflammatory factors downstream of TBK1/NF-κB including *Ccl4*, *Ccl5*, *Cxcl10*, and type I IFN-related genes *Isg15* and *Ifnb* were increased significantly in WT BMDMs after ACS exposure (Figure 4*C*–*G*). As with the TBK1/NF-κB pathway itself, we noted that *Usp25*$^{-/-}$ BMDMs showed higher inductions of inflammatory factors when exposed to ACS compared with WT BMDMs. Moreover, IFNβ protein levels were found to be increased in *Usp25*$^{-/-}$ BMDMs compared with WT BMDMs (Figure 4*H*). These results may indicate that acinar cell death releases factors that activate TBK1/NF-κB in macrophages, and that USP25 may regulate TBK1/NF-κB through a STING-independent mechanism.

Because we used a *Usp25*$^{-/-}$ model with precise temporal regulation, there is a possibility that some of the effects noted may be owing to utilization of alternate signaling pathways. In an attempt to overcome this limitation, we restored *Usp25* in BMDMs harvested from *Usp25*$^{-/-}$ mice, and measured the activation of the TBK1/NF-κB pathway after ACS exposure. Our results show that expression of Usp25 in *Usp25*$^{-/-}$ BMDMs largely reverses ACS-induced phosphorylation of TBK1, IRF3, and P65 (Figure 5*A*). *Usp25* expression also prevented NF-kappa-B inhibitor alpha degradation, another measure of reduced NF-κB activity (Figure 5*A*). Furthermore, Usp25 expression reduced the level of *Ccl4* and *Ifnb* induction in cells after ACS exposure (Figure 5*C*–*G*). However, no reductions were seen in *Ccl5*, *Cxcl10*, and *Isg15* in cells transfected with *Usp25* vector compared with control vector. These results suggest that exaggerated inflammatory responses seen in *Usp25*$^{-/-}$ BMDMs is owing to *Usp25* deficiency.

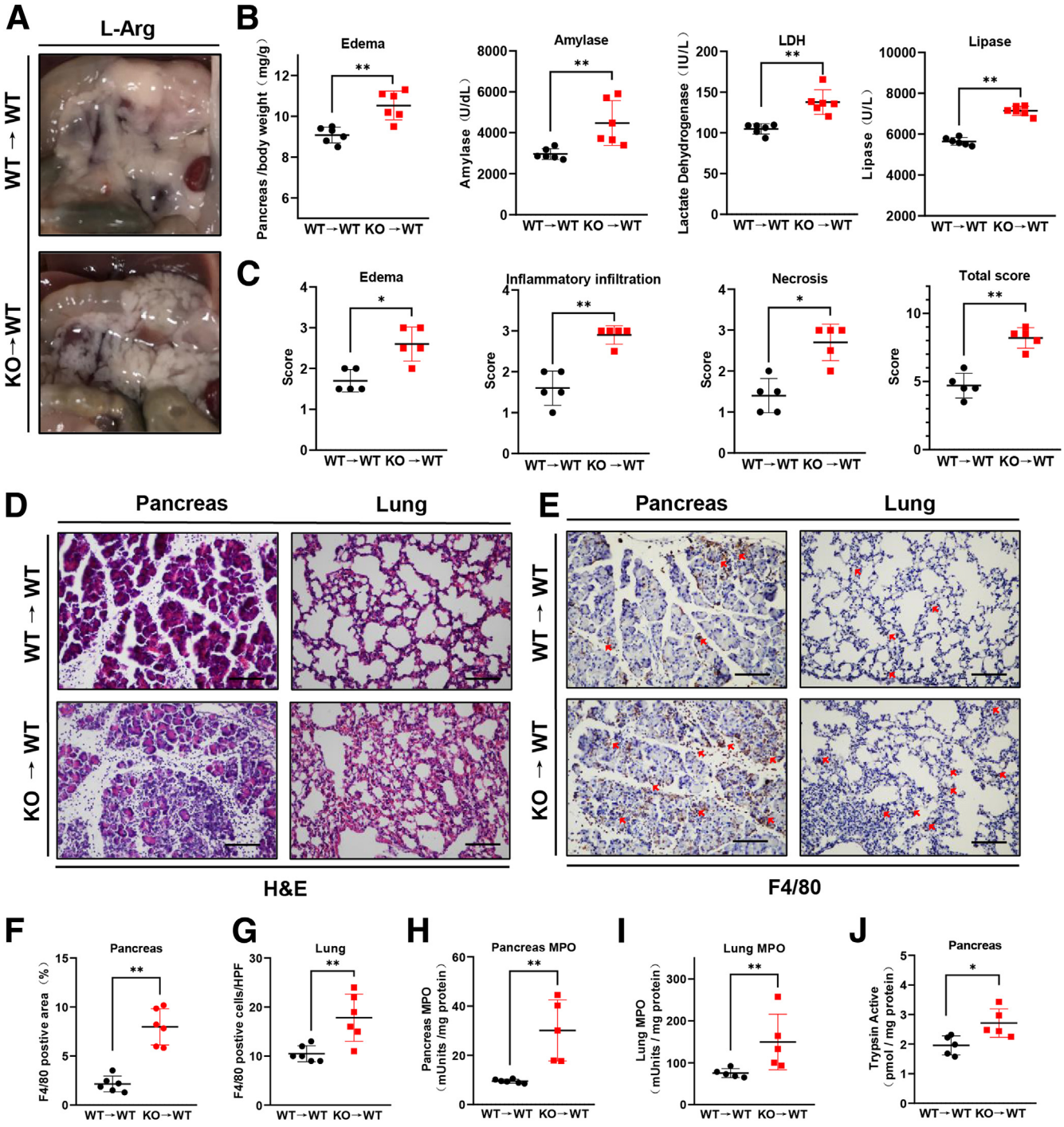

Figure 3. Deficiency in macrophage-expressed *Usp25* worsens L-arginine–induced pancreatitis. WT mice were irradiated and reconstituted with bone marrow from either WT (WT→WT) or Usp25$^{-/-}$ (KO→WT) mice. Mice then were subjected to a L-arginine–induced model of pancreatitis. (*A*) Gross morphology of the pancreas 72 hours after L-arginine administration. (*B*) Pancreas-to-body-weight ratios, and serum levels of amylase, LDH, and lipase in mice. (*C*) Histopathologic scoring of pancreas tissues. (*D*) Representative H&E-stained images of pancreas and lung tissues. *Scale bar*: 100 μm. (*E*) Representative immunohistochemical staining images showing F4/80 in the pancreas and lung tissues. *Red arrows* indicate positive staining. *Scale bar*: 100 μm. (*F* and *G*) Quantification of F4/80 staining area in (*F*) pancreas and (*G*) lung. (*H* and *I*) MPO activity in the (*H*) pancreas and (*I*) lung. (*J*) Trypsin activity in the pancreas. Data are shown as means ± SD; n = 5–6. *$P < .05$ and **$P < .01$. HPF, high-power field.

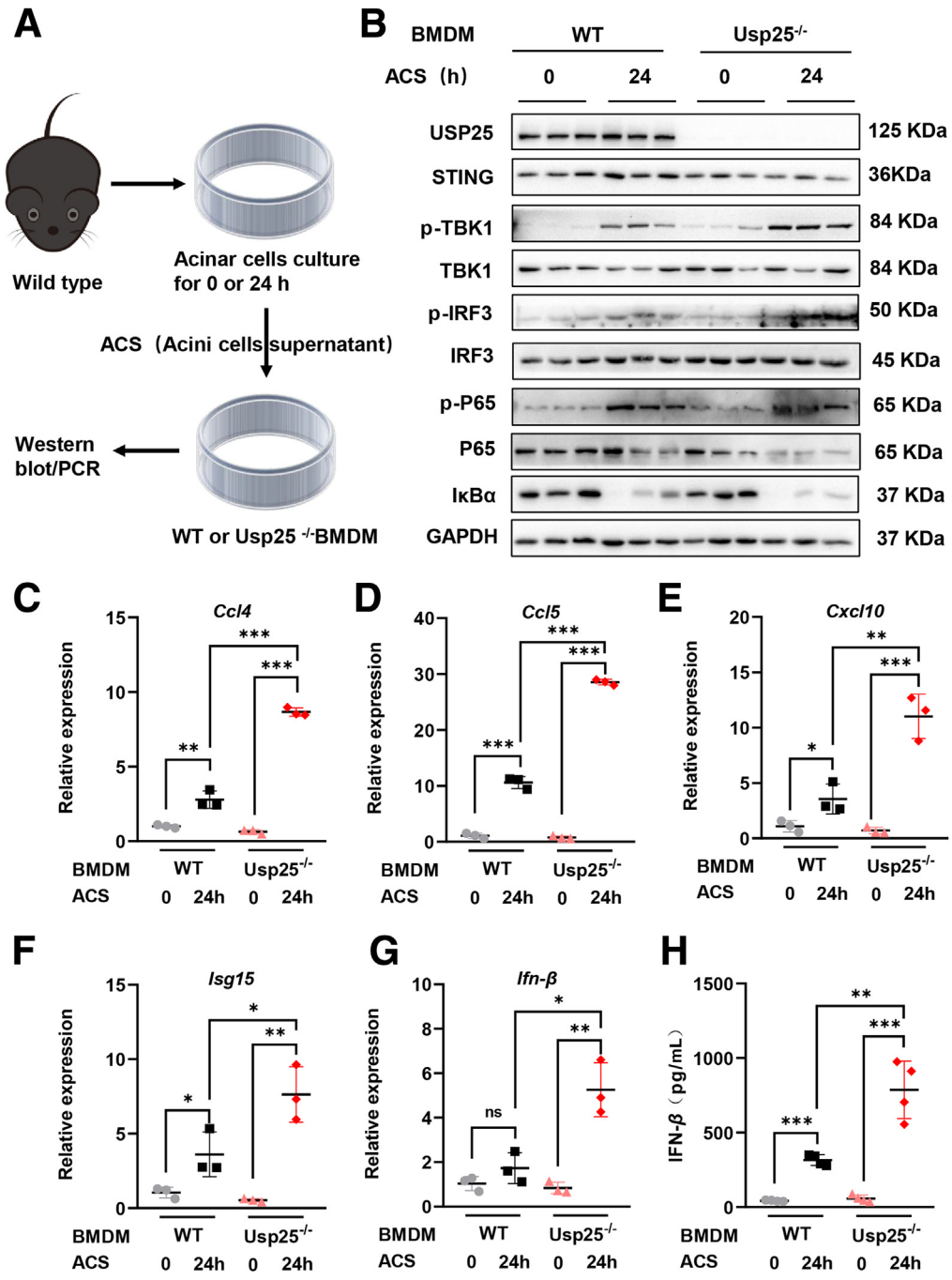

Figure 4. BMDMs from *Usp25*$^{-/-}$ mice show enhanced inflammatory responses. (*A*) Schematic illustration of the experimental model. Acinar cells were isolated from mice and cultured for 0 or 24 hours. ACS was collected and applied to BMDMs harvested from WT and *Usp25*$^{-/-}$ mice. BMDM responses then were measured. (*B*) BMDMs from WT and *Usp25*$^{-/-}$ mice were exposed to ACS for 60 minutes. Cell lysates were probed for downstream signaling proteins by immunoblotting. (*C*–*G*) Messenger RNA levels of inflammatory factors in BMDMs from WT and *Usp25*$^{-/-}$ mice that were exposed to ACS for 9 hours. (*H*) BMDMs were exposed to ACS for 18 hours, and IFNβ levels in culture medium were determined. (*C*–*H*) Data are shown as means ± SD; n = 3 independent experiments. **P* < .05, ***P* < .01, and ****P* < .001. GAPDH, glyceraldehyde-3-phosphate dehydrogenase; p-IRF3, phosphorylated interferon regulatory factor 3; p-P65, phosphorylated P65 protein; p-TBK1, phosphorylated TANK binding kinase 1; PCR, polymerase chain reaction.

Involvement of STING in AP has been reported previously and studies have shown that STING activation by Dimethylxanthine acetic acid (DMXAA) worsens AP through activation of downstream pathways.[12] We exposed WT and *Usp25*$^{-/-}$ BMDMs to DMXAA and examined the downstream pathways. Interestingly, *Usp25*$^{-/-}$ BMDMs showed increased phosphorylated TBK1, IRF3, and P65 proteins compared with WT BMDMs when exposed to DMXAA (Figure 5*B*). Similarly, DMXAA increased messenger RNA levels of *Ccl4*, *Ccl5*, *Cxcl10*, *Isg15*, and *Ifnb* in WT BMDMs, which were increased further in DMXAA-treated *Usp25*$^{-/-}$ BMDMs (Figure 5*H*–*L*). These data indicate that *Usp25* deficiency in macrophages exacerbates inflammatory responses, potentially through enhanced TBK1/NF-κB signaling.

Usp25$^{-/-}$ Mice Show Exaggerated TBK1/NF-κB Activation in the L-Arginine–Induced Severe AP Model

Based on our culture studies showing that *Usp25*$^{-/-}$ BMDMs activate TBK1/NF-κB in response to ACS, we probed for TBK1/NF-κB activation and downstream cytokine

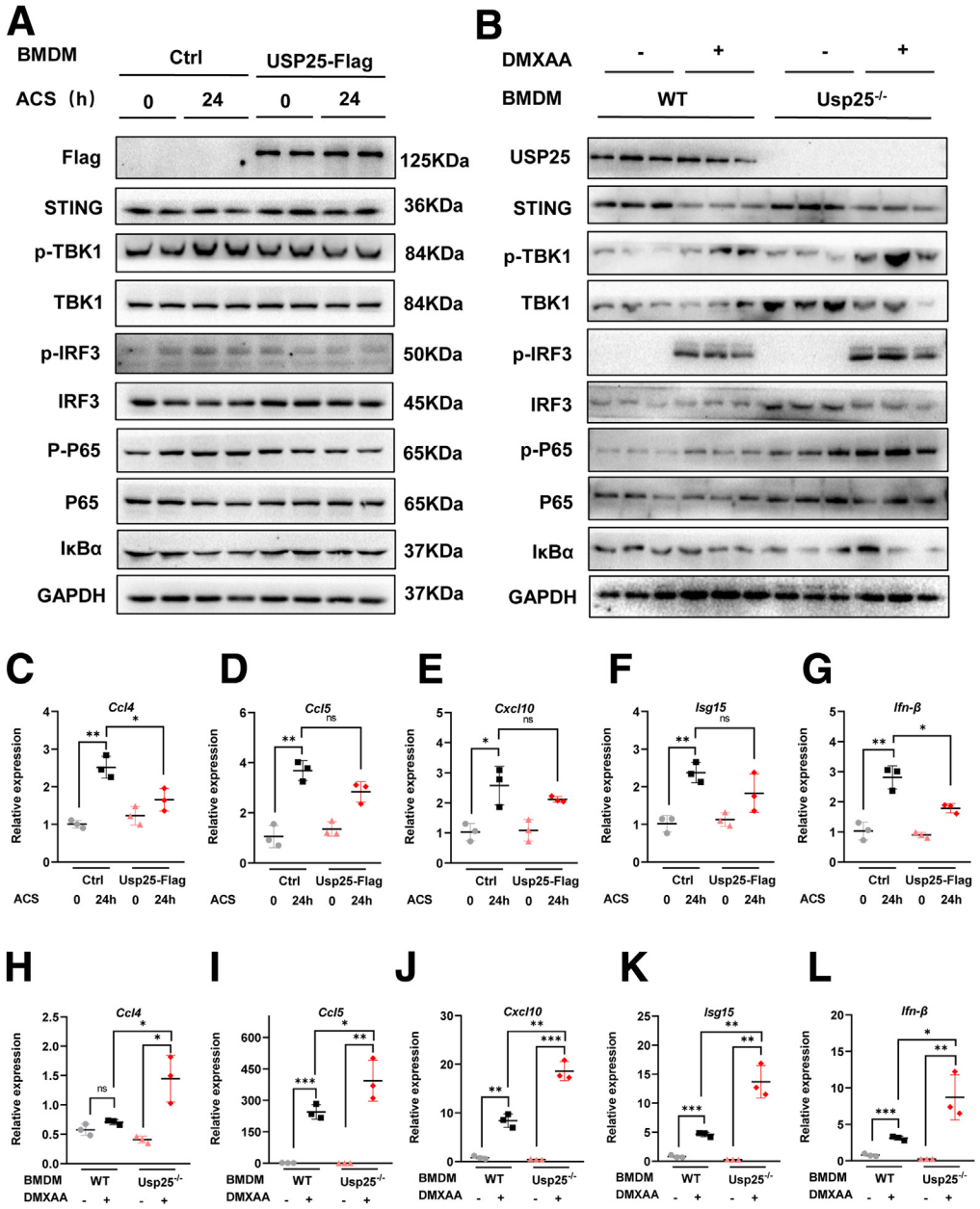

Figure 5. Expression of USP25 in *Usp25*$^{-/-}$ BMDMs reverse ACS-induced inflammatory responses in cells and STING agonist activates downstream signaling in both WT and *Usp25*-deficient macrophages. *Usp25*$^{-/-}$ BMDMs were transfected with control plasmid or plasmid expressing Flag-tagged *Usp25* (NM_013918; Genechem). Acinar cells were isolated from WT mice and cultured for 0 or 24 hours. ACS collected from 0 or 24 hours was applied to control- and *Usp25*-plasmid–transfected BMDMs. (*A*) ACS exposure of BMDMs was performed for 60 minutes. Lysates then were probed for activation of downstream inflammatory response proteins. Antibody against Flag was used to detect USP25 expression. (*B*) BMDMs were prepared from WT and *Usp25*$^{-/-}$ mice. Cells were treated with 40 μg/mL STING agonist DMXAA or vehicle for 1 hour. Lysates then were probed for activation of downstream inflammatory response proteins. Total proteins and glyceraldehyde-3-phosphate dehydrogenase (GAPDH) were used as control. (*C–G*) ACS exposure was called out for 9 hours. Messenger RNA levels of inflammatory factors then were measured by quantitative polymerase chain reaction. (*H–L*) BMDMs were treated with DMXAA for 9 hours. Messenger RNA levels of inflammatory factors then were measured. (*C–L*) Data are shown as means ± SD; n = 3. **P* < .05, ***P* < .01 and ****P* < .001. Ctrl, control; p-IRF3, phosphorylated interferon regulatory factor 3; p-P65, phosphorylated P65 protein; p-TBK1, phosphorylated TANK binding kinase 1.

expression in the L-arginine–induced mouse model of AP, including the bone marrow chimeric mice. Pancreatic tissues showed that USP25 protein levels are significantly lower in KO→WT mice upon L-arginine administration compared with WT→WT mice (Figure 6*A*). Levels of STING also were found to be lower in the KO→WT mice. However, downstream factors, including Phosphorylated-TBK1, Phosphorylated-IRF3, and Phosphorylated-P65 all were significantly higher in KO→WT mice compared with WT→WT mice (Figure 6*A*). As expected from these results, *Ccl4*, *Ccl5*, *Cxcl10*,

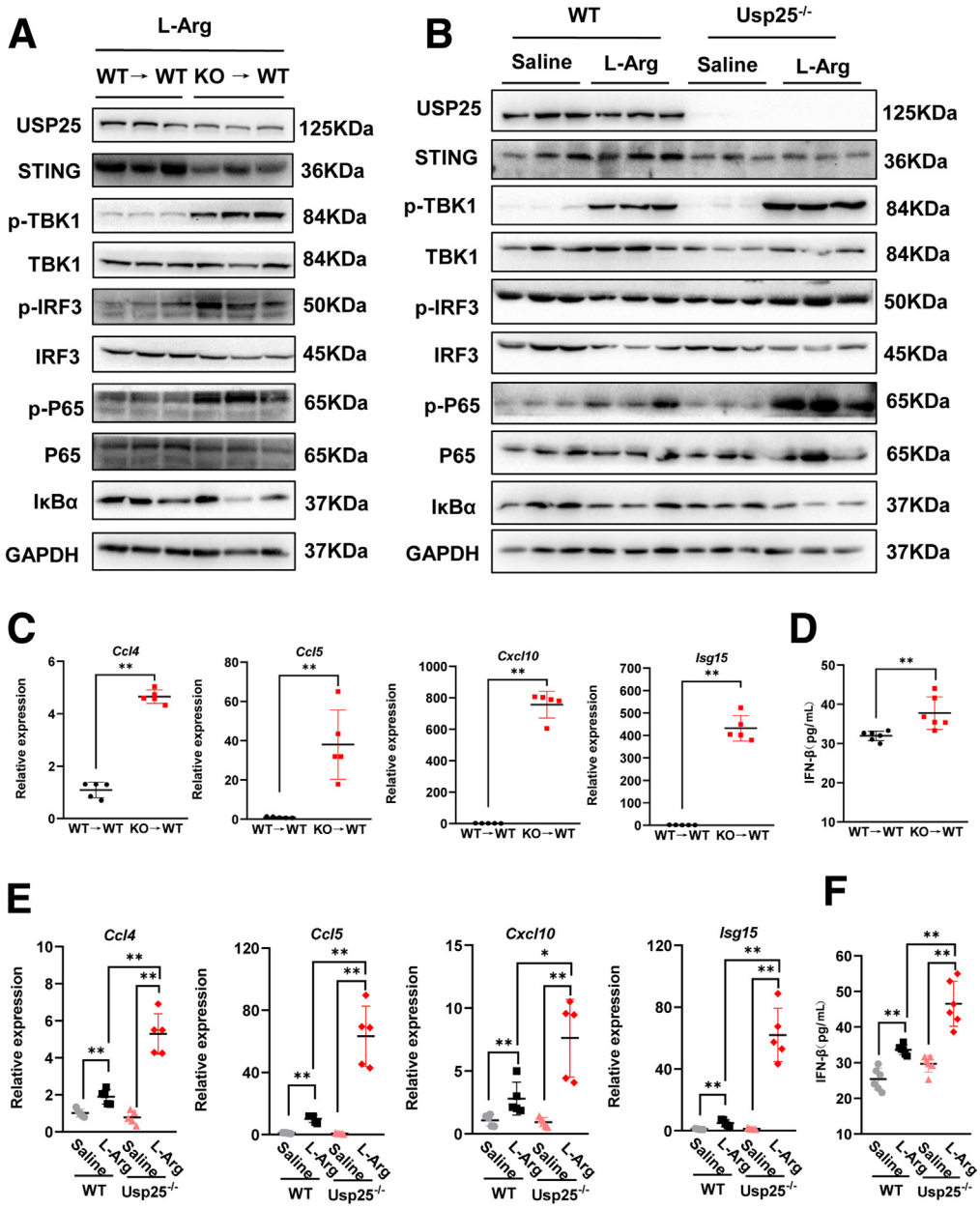

Figure 6. BMDMs deficient in *Usp25* show enhanced inflammatory responses to L-arginine. (*A*) Bone marrow of WT mice was irradiated and reconstituted with bone marrow cells from either WT mice (WT→WT) or *Usp25*$^{-/-}$ mice (KO→WT). Mice then were challenged with L-arginine to induce pancreatitis. Pancreatic lysates were probed for inflammatory pathway activation by immunoblotting. (*B*) WT and *Usp25*$^{-/-}$ mice were injected with saline or L-arginine. Pancreatic lysates were used for immunoblotting. (*C*) Messenger RNA levels of *Ccl4*, *Ccl5*, *Cxcl10*, and *Isg15* in the pancreas of mice. (*D*) Serum IFNβ levels were measured by ELISA. (*E*) Messenger RNA levels of *Ccl4*, *Ccl5*, *Cxcl10*, and *Isg15* in the pancreas of WT and *Usp25*$^{-/-}$ mice. (*F*) Serum IFNβ levels in mice. (*C–F*) Data are shown as means ± SD; n = 5–6. $^{*}P < .05$ and $^{**}P < .01$. GAPDH, glyceraldehyde-3-phosphate dehydrogenase; p-IRF3, phosphorylated interferon regulatory factor 3; p-P65, phosphorylated P65 protein; p-TBK1, phosphorylated TANK binding kinase 1.

and *Isg15* (Figure 6*C*) and serum IFNβ (Figure 6*D*) were significantly higher in the pancreatic tissues of KO→WT mice compared with WT→WT mice. Analysis of tissues from WT and *Usp25*$^{-/-}$ mice (without bone marrow reconstitution) showed the expected readouts: decreased STING levels, increased TBK1/NF-κB activity, and significantly induced levels of inflammatory factors (Figure 6*B*, *E*, and *F*). Furthermore, we found that the well-established NF-κB inhibitor BAY11-7082 decreased pancreatic injury in *Usp25*$^{-/-}$ mice in response to L-arginine (Figure 7*A* and *B*). A protective effect of BAY11-7082 also was observed in histopathologic examination of pancreatic tissues from *Usp25*$^{-/-}$ mice (Figure 7*C* and *D*). These data, at a minimum, support the involvement of NF-κB in exaggerated AP phenotype observed in *Usp25*$^{-/-}$ mice challenged with L-arginine.

Usp25$^{-/-}$ Mice Show Exacerbated Cerulein-Induced Pancreatitis and Associated Lung Injury

No experimental model of AP is perfect, and different models offer different advantages and disadvantages. One of the most widely used model of AP is induced by repetitive injections of cerulein.[25] This treatment reliably generates mild, edematous pancreatitis in C57BL/6J mice when administered in 6–10 intraperitoneal injections.[25] To bolster our finding that *Usp25* deficiency worsens AP, we challenged WT and *Usp25*$^{-/-}$ mice with 8 cerulein injections given at hourly intervals. First, to examine the effects of USP25 deletion soon after developing cerulein-induced pancreatitis, lungs and pancreas were harvested from mice at different time points, including 9, 13, and 17 hours after the first cerulein injection (data not shown). Our data

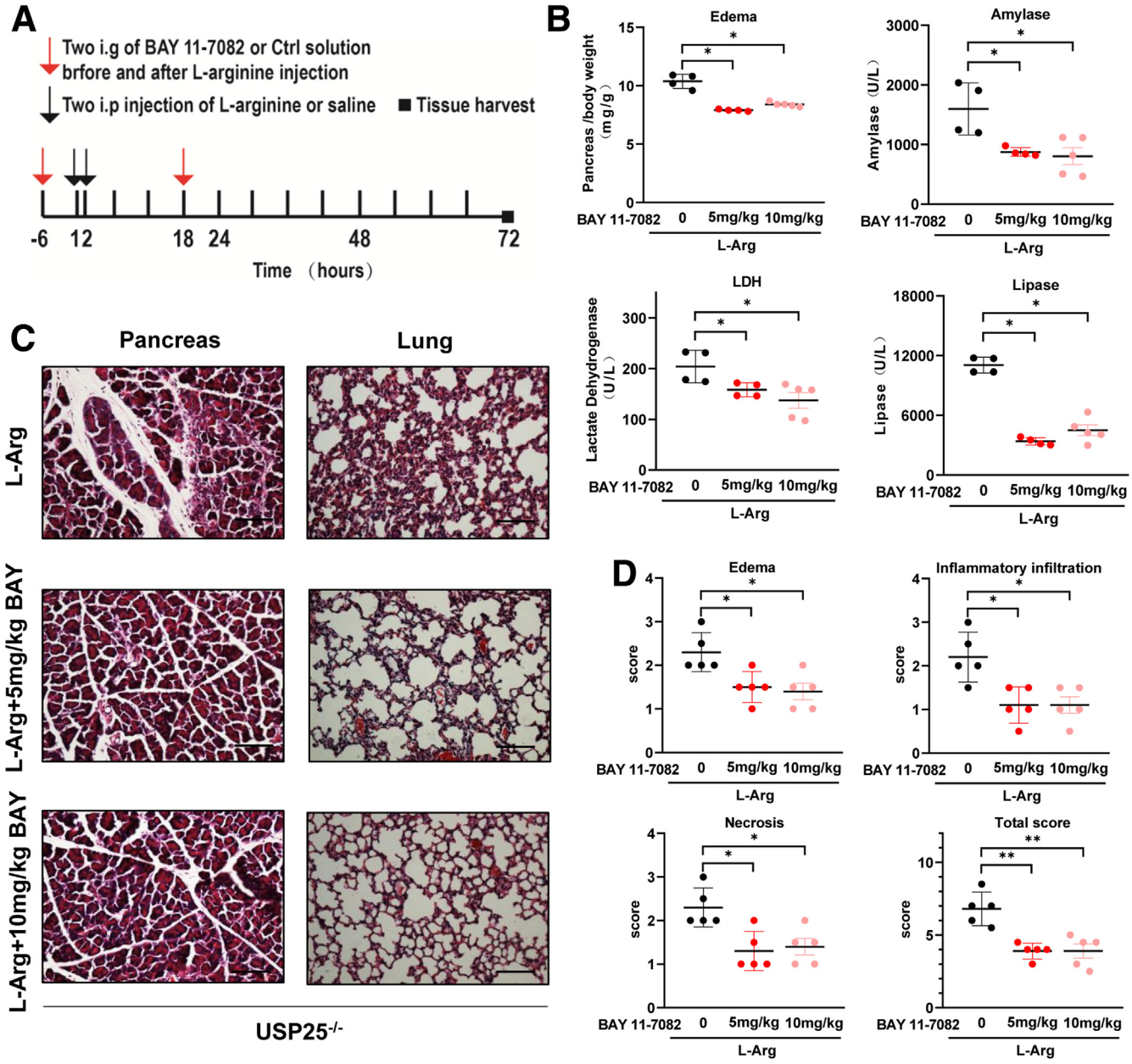

Figure 7. NF-κB inhibitor suppresses L-arginine (L-Arg)-induced pancreatitis in *Usp25*$^{-/-}$ mice. (*A*) Schematic illustration of the model. *Usp25*$^{-/-}$ mice received BAY 11-7082, a NF-κB inhibitor, at 5 or 10 mg/kg. Control mice received vehicle alone. Six hours later, mice received 2 injections of L-arginine with a 1-hour interval between. Finally, mice received another dose of BAY 11-7082, 6 hours after the last L-arginine injection. Pancreas and lungs were harvested from mice and examined for tissue injury. (*B*) Pancreas-to-body-weight ratios, and levels of serum amylase, LDH, and lipase in mice. (*C*) Representative H&E-stained images of pancreas and lung tissues in mice at the experimental end point. *Scale bar*: 100 μm. (*D*) Histopathologic assessment of edema, inflammatory cell infiltration, necrosis, and total pancreatic injury in mice. (*B* and *D*) Data are shown as means ± SD; n = 4–5. **P* < .05, ***P* < .01. Ctrl, control; i.g, intragastric; i.p, intraperitoneal.

show that cerulein challenge caused pancreatic injury that was evident at the 9-hour time point. Even though both lung and pancreas tissues recovered at 13 and 17 hours, it was not a full recovery when compared with saline-injected *Usp25*$^{-/-}$ mice (data not shown). At a later time point, gross morphologic examination showed white and enlarged pancreas in cerulein-challenged *Usp25*$^{-/-}$ mice, indicating edema (Figure 8*A*). Histologic analysis and subsequent injury scoring showed that *Usp25* deficiency increases edema and inflammatory cell infiltration after cerulein administration compared with mice with intact *Usp25* (Figure 8*B* and *C*). The level of necrosis, however, was not statistically different between WT and *Usp25*$^{-/-}$ mice. Biochemical assays showed higher serum amylase, lipase, and LDH levels in *Usp25*$^{-/-}$ mice in response to cerulein administration compared with WT mice (Figure 8*D*).

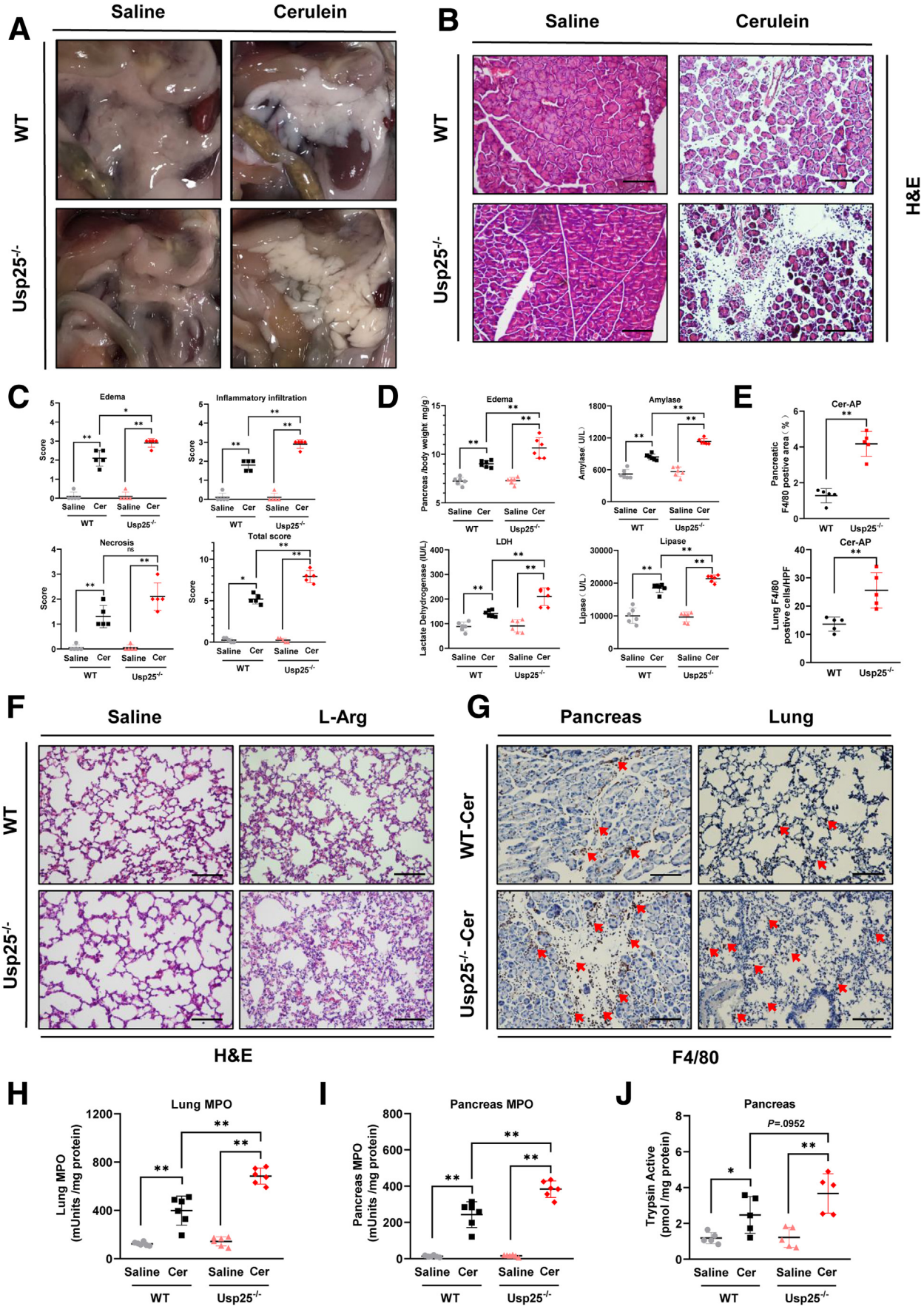
A
Saline
Cerulein
WT
Usp25-/-
B
Saline
Cerulein
WT
Usp25-/-
H&E
C
Edema
Inflammatory infiltration
Necrosis
Total score
Score
Saline Cer
WT
Usp25-/-
D
Edema
Amylase
LDH
Lipase
Pancreas /body weight mg/g
Amylase U/L
Lactate Dehydrogenase (IU/L)
Lipase (U/L)
E
Cer-AP
Pancreatic F4/80 postive area (%)
Lung F4/80 postive cells/HPF
F
Saline
L-Arg
WT
Usp25-/-
H&E
G
Pancreas
Lung
WT-Cer
Usp25-/--Cer
F4/80
H
Lung MPO
Lung MPO (mUnits /mg protein)
I
Pancreas MPO
Pancreas MPO (mUnits /mg protein)
J
Pancreas
P=.0952
Trypsin Active (pmol /mg protein)

Lung tissues harvested from mice after cerulein challenge showed more tissue damage in *Usp25*$^{-/-}$ mice compared with WT mice (Figure 8*F*). We then evaluated macrophage infiltration in pancreas and lung sections using F4/80 immunohistochemistry staining, as performed in the L-arginine model. A greater F4/80-stained lung and pancreas area was observed in *Usp25*$^{-/-}$ mice (Figure 8*E* and *G*). Similarly, MPO activity in the lung and pancreas (Figure 8*H* and *I*) was higher in *Usp25*$^{-/-}$ mice compared with WT mice after cerulein injections. Furthermore, the trypsin activity in the pancreas was higher in the *Usp25*$^{-/-}$ mice (Figure 8*J*). Collectively, these data confirm that *Usp25* deficiency also aggravates cerulein-induced pancreatitis, as observed in L-arginine–induced pancreatitis.

Usp25$^{-/-}$ Mice Also Show Exaggerated Diet-Induced Pancreatitis

We next used a diet-induced model of pancreatitis to confirm the role of USP25. A CDE has been shown to produce necrotizing pancreatitis with hemorrhage in young female mice.[12,26] For this model, 4-week-old female WT and *Usp25*$^{-/-}$ mice were given a CDE or standard rodent chow (chow diet [CD]; control) diet for 72 hours. We found obvious signs of edema in WT and *Usp25*$^{-/-}$ mice fed a CDE (Figure 9*A*). Quantitative assessment of pancreatic injury showed that *Usp25*$^{-/-}$ deficiency worsens CDE-induced pancreatitis in mice (Figure 9*B* and *C*). Lung histopathology and MPO activity in lung and pancreatic tissues of mice also showed exaggerated responses in *Usp25*$^{-/-}$ mice compared with WT mice (Figure 9*D*–*F*). In addition, pancreatic trypsin activity levels were significantly higher in *Usp25*$^{-/-}$ mice after CDE feeding (Figure 9*G*).

A slightly modified CDE model was used to assess survival in mice. *Usp25*$^{-/-}$ and WT mice were fasted for 12 hours and fed a CDE for 4 days, followed by normal diet for another 4 days. *Usp25*$^{-/-}$ mice fed a CDE appeared to have a poorer prognosis compared with WT mice (Figure 9*H*). However, the results did not reach statistical significance ($P = .1215$).

The Role of USP25 in AP Is Independent of the Associations With TLR4 and Tumor Necrosis Factor–Receptor–Associated Factor

USP25 is a deubiquitinating enzyme. Activity of this protein has been implicated in human diseases, including cancers and various inflammatory conditions.[27,28,29] The molecular mechanisms by which USP25 participates may vary depending on the disease. Some of the reported mechanisms include regulation of suppressor of cytokine signaling 3-Phosphorylated signal transducer and activator of transcription 3, Wnt pathway/β-catenin, and NF-κB and c-Jun-N-terminal kinase (JNK) signaling pathways.[27,28,30,29] A recent report showed that USP25 inhibited Toll-like receptor 4 (TLR4)-triggered proinflammatory signaling and promoted type I interferon signaling through deubiquitination of tumor necrosis factor receptor–associated factor (TRAF)3.[31] These researchers also found that USP25 associates with TRAF3 and TRAF6 after viral infection and protects against proteasome-dependent or -independent degradation of TRAF3 and TRAF6.[22] To explore whether this mechanism is at play in AP, we probed for the levels of TLR4, TRAF3, and TRAF6 in BMDMs harvested from WT and *Usp25*$^{-/-}$ mice after ACS exposure. ACS exposure did not change the expression of TLR4 or TRAF3 in either WT or *Usp25*$^{-/-}$ BMDMs (Figure 10*A*). The levels of TRAF6, however, were suppressed in both WT and *Usp25*$^{-/-}$ BMDMs in response to ACS. Expression of *Usp25* in *Usp25*$^{-/-}$ BMDMs failed to restore TRAF6 levels after ACS treatment (Figure 10*B*). Analysis of pancreatic tissues of WT and *Usp25*$^{-/-}$, and chimeric KO→WT and WT→WT mice did not show any changes in TLR4, TRAF3, or TRAF6 expression after L-arginine challenge (Figure 10*C* and *D*). These results indicate that the involvement of USP25 in AP may be independent of the known associations with TLR4 and TRAF proteins.

The Role of USP25 in AP Is Not Caused by the Modulation of Interleukin 17

Zhong et al[32] identified USP25 as a negative regulator of interleukin (IL)17-mediated signaling and showed that *Usp25*$^{-/-}$ mice show a greater sensitivity to IL17-dependent inflammation and autoimmunity. Because IL17 has been shown to participate in AP pathogenesis,[29,33] we wondered if the anti-inflammatory effects of USP25 were mediated through the modulation of the IL17 pathway. Surprisingly, when compared with the WT BMDMs, transcript levels of *Il17a* and downstream *Ccl7*, *Ccl20*, *Cxcl5*, *Tnf*, and *Cxcl1* were not increased significantly in ACS- or IL17A-exposed *Usp25*$^{-/-}$ BMDMs (Figure 11*A* and *B*). In addition, there was no significant change in mitogen activated kinase-like protein pathway activation, as assessed by phosphorylated protein levels, between WT and *Usp25*$^{-/-}$ BMDMs upon IL17A stimulation (Figure 11*C*). We also evaluated the levels of NF-κB signaling proteins in WT and *Usp25*$^{-/-}$ BMDMs after IL17A exposure. Interestingly, IL17A did not induce NF-κB activation in either WT or *Usp25*$^{-/-}$ BMDMs when tested up to 45 minutes (data not shown). These new data suggest that the effects of USP25 seen in our experimental platform are not caused by the modulation of IL17.

Figure 8. (***See previous page***). ***Usp25*$^{-/-}$ mice show aggravated cerulein (Cer)-induced AP.** (*A*) Gross morphology of pancreas after cerulein-induced pancreatitis. (*B*) Representative H&E-stained images of pancreatic tissues. *Scale bar*: 100 μm. (*C*) Levels of pancreatic edema, inflammatory cell infiltration, necrosis, and total injury score in pancreas of cerulein-induced pancreatitis in mice. (*D*) Pancreas-to-body-weight ratios, and serum levels of amylase, LDH, and lipase in WT and *Usp25*$^{-/-}$ mice. (*E*) pancreas and lung were stained for macrophage marker F4/80. Quantitative measurement of F4/80 immunoreactivity is shown. (*F*) Representative H&E-stained images of lung tissue. *Scale bar*: 100 μm. (*G*) F4/80 staining in the pancreas and lung tissues of WT and *Usp25*$^{-/-}$ mice after cerulein-induced AP. *Arrows* indicate positive staining. *Scale bar*: 100 μm. MPO activity in the (*H*) lung and (*I*) pancreas of mice. (*J*) Trypsin activity in pancreas of mice. (*C–E* and *H–J*) Data are shown as means ± SD; n = 5–6. **P* < .05 and ***P* < .01.

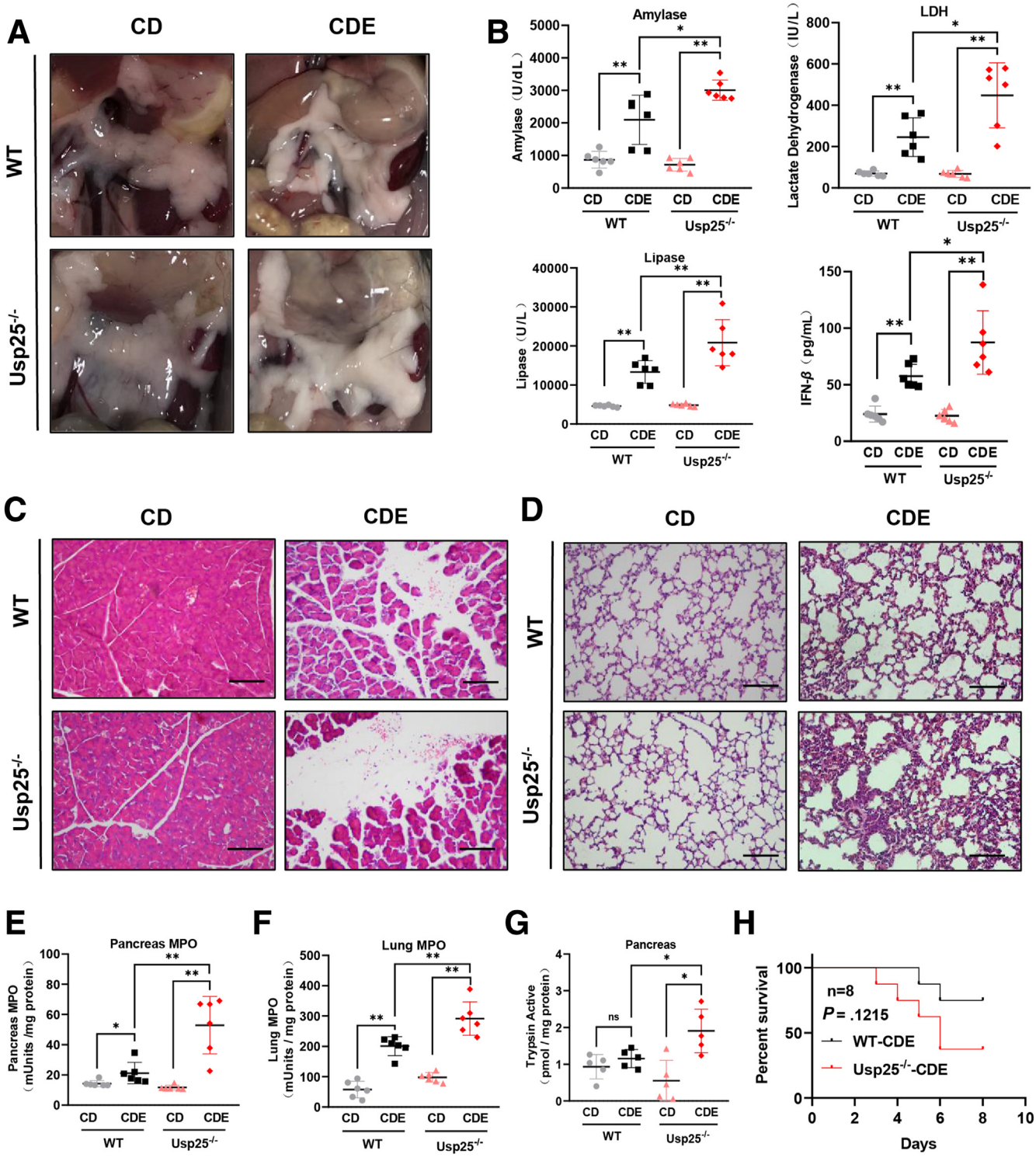

Figure 9. Exaggerated responses to CDE-induced pancreatitis in *Usp25*$^{-/-}$ mice. (*A*) Gross morphology of pancreatic tissues in WT and *Usp25*$^{-/-}$ mice after 72-hour CDE feeding. Control diet included standard rodent chow diet (CD). (*B*) Serum amylase, LDH, lipase, and IFNβ levels in CD- or CDE-fed WT and *Usp25*$^{-/-}$ mice. (*C*) Representative H&E-stained images of pancreas in mice. *Scale bar*: 100 μm. (*D*) Representative H&E-stained images of lung tissues in mice. *Scale bar*: 100 μm. (*E* and *F*) MPO activity in the (*E*) pancreas and (*F*) lung of CD- or CDE-fed WT and *Usp25*$^{-/-}$ mice. (*G*) Trypsin activity in the pancreas from CD or CDE-fed WT and *Usp25*$^{-/-}$ mice. (*H*) Survival rate in WT and *Usp25*$^{-/-}$ mice fed a CDE or control CD diet. (*B* and *E–G*) Data are shown as means ± SD; n = 5–6. **P* < .05 and ***P* < .01. (*H*) n = 8.

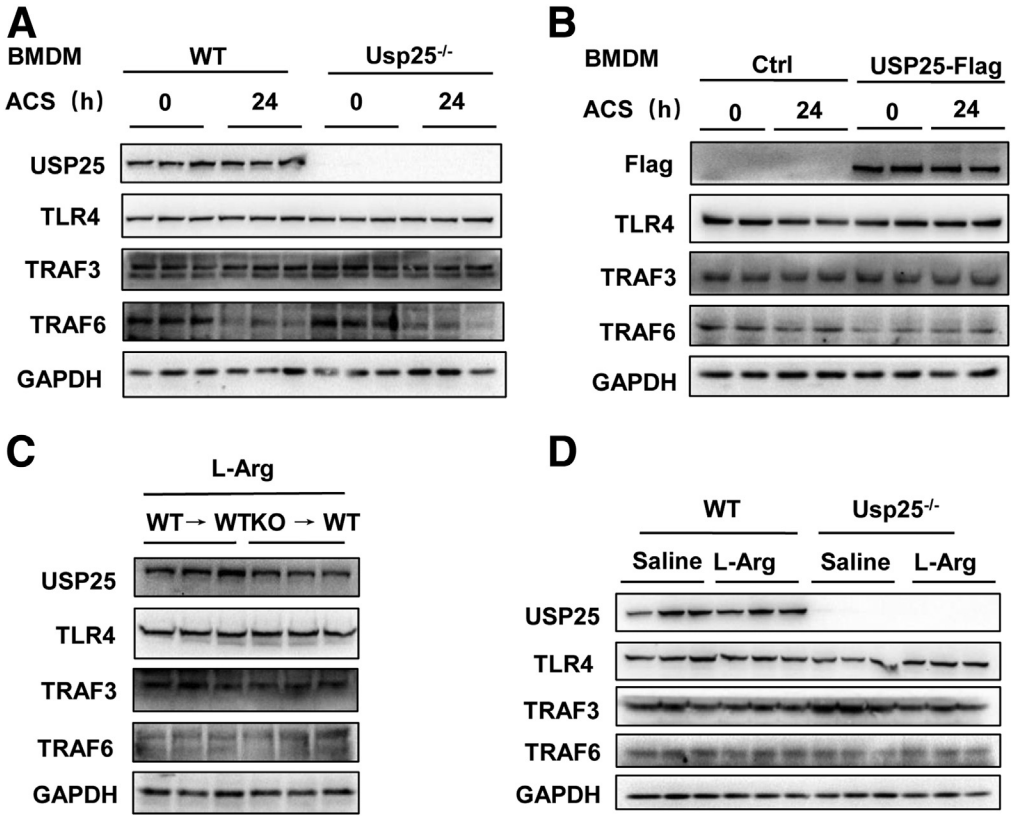

Figure 10. The effect of *Usp25* deletion in macrophages on the expression of TRAF and TLR4. BMDMs were prepared from WT and *Usp25*$^{-/-}$ mice. Acinar cells were isolated from WT mice and cultured for 0 or 24 hours. ACS collected from 0 or 24 hours was applied to BMDMs. (*A*) BMDMs were exposed to ACS for 60 minutes. Lysates were collected and immunoblotted for the expression of TRAF3, TRAF6 and TLR4. (*B*) BMDMs from *Usp25*$^{-/-}$ mice were transfected with control or *Usp25* expressing plasmid. Cells then were exposed to ACS for 60 minutes. Levels of TRAF and TLR4 proteins were detected by immunoblotting. (*C*) WT mice were irradiated and reconstituted with bone marrow cells derived from either WT (WT→WT) donor mice or *Usp25*$^{-/-}$ mice (KO→WT). Mice then were challenged with L-arginine. Pancreas was harvested and levels of TLR4 and TRAF were detected in tissue lysates. (*D*) WT and *Usp25*$^{-/-}$ mice were challenged with L-arginine. Lysates from pancreas were used for immunoblotting. GAPDH, glyceraldehyde-3-phosphate dehydrogenase.

Discussion

Our study discovered a novel role of USP25 in AP. Comprehensive cell culture and mouse modeling studies showed that *Usp25* deficiency worsens AP. Specifically, our studies show that *Usp25*$^{-/-}$ mice show exaggerated pancreatic injury induced by L-arginine, cerulein, or CDE feeding over WT mice. Without Usp25, increased inflammatory cell infiltration, inflammatory cytokine levels, and necrosis is evident. This worsening of AP presentation likely was mediated by the lack of *Usp25* in macrophages. We tested this idea by reconstituting the bone marrow of WT mice with *Usp25*$^{-/-}$-derived marrow cells and show that these chimeric mice mimic global *Usp25*-deficient mice. We then used primary macrophages derived from mice and showed that cells lacking *Usp25* have an enhanced TBK1/NF-κB response when challenged with acinar cell factors or L-arginine.

There are many causes of AP. However, all leads trigger the same pathologic pathways and cellular dysfunction that culminate in acinar cell damage and local and systemic inflammation. Damaged acinar cells recruit various immune cells such as neutrophils, monocytes, and macrophages by releasing cytokines, chemokines, and expressing adhesion molecules.[7,11,34] When immune cells migrate to these sites, the interaction between necrotic pancreatic tissue and immune cells, such as neutrophils and macrophages, further promotes local and systemic inflammatory responses, ultimately leading to organ injury.[35,36] Neutrophil infiltration occurs in the early stages of AP, and neutrophil extracellular traps can cause duct blockage, activate proinflammatory signaling, and activate trypsinogen prematurely.[37–39] Macrophages also play key roles in local and systemic inflammation responses at the onset of AP.[40–42] Classically polarized M1 macrophages dominate in the proinflammatory phase of AP, while M2-like macrophages dominate the repair/regenerative phase.[41] Upon acinar cell necrosis, released proinflammatory mediators and chemokines, as well as damage-associated molecular patterns, activate TLRs and inflammasome complexes in macrophages that may exacerbate pancreatic injury.[43–45] Recently, it was reported that inhibition of C-C motif chemokine ligand 2-induced macrophage migration and blockade of

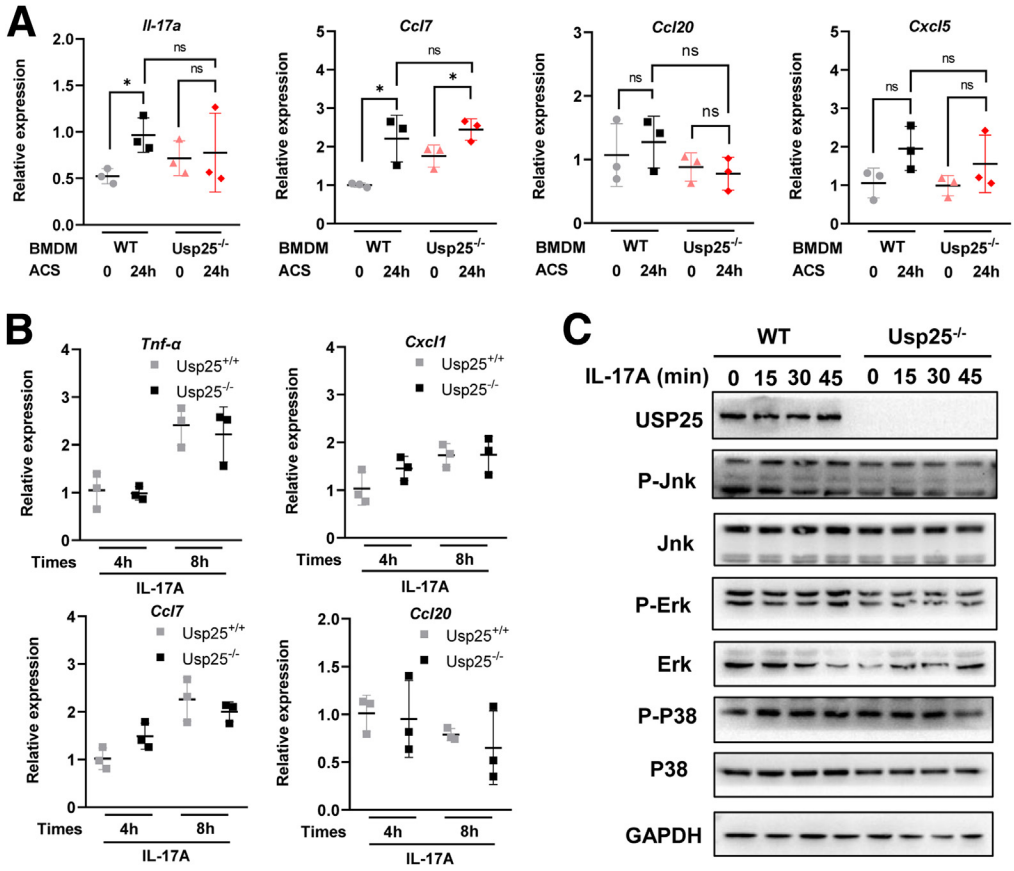

Figure 11. Enhanced inflammatory responses after *Usp25* deletion in macrophages are independent of IL17 signaling. (*A*) BMDMs were prepared from WT and *Usp25*$^{-/-}$ mice. Acinar cells were isolated from WT mice and cultured for 0 or 24 hours. ACS collected from 0 or 24 hours was applied to BMDMs for 9 hours. Messenger RNA levels of *Il17a*, *Ccl7*, *Ccl20*, and *Cxcl5* were measured. (*B*) BMDMs from WT or *Usp25*$^{-/-}$ mice were treated with IL17A at 50 ng/mL for 4 or 8 hours. Messenger RNA levels of *Tnf*, *Cxcl1*, *Ccl7*, and *Ccl20* were measured. (*C*) BMDMs from WT or *Usp25*$^{-/-}$ mice were treated with IL17A at 100 ng/mL for up to 45 minutes. Levels of USP25 and phosphorylated mitogen-activated protein kinase (JNK, ERK, p38) were determined using Western blot. The total levels of mitogen-activated protein kinase proteins and glyceraldehyde-3-phosphate dehydrogenase (GAPDH) were used as control. (*A* and *B*) Data are shown as means ± SD; n = 3. *$P < .05$. P-Erk, phosphorylated extracellular signal-regulated kinase; P-JNK, phosphorylated c-jun N-terminal kinase; P-P38, phosphorylated p38 MAPK.

cytokine signaling 3–dependent activation of macrophages can prevent the progression of AP and distant organ failure.[46] Furthermore, a single-cell mass cytometry analysis has shown that a dynamic shift in pancreatic CD206^{+} macrophage population is observable during AP and recovery.[47] Our study adds to the importance of macrophages in AP progression and shows that *Usp25* deficiency in macrophages exacerbates L-arginine–induced AP and promoted macrophage infiltration into pancreas and lung. These findings are in line with previous studies showing that overexpression of USP25 reduces LPS-induced macrophage activation and inflammatory cytokines production.[20] Moreover, *Usp25* knockdown has been shown to generate proinflammatory effects in Kupffer cells.[48] Taken together, these studies indicate that increasing Usp25 activity may counter inflammatory responses in AP.

Our data suggest that the effects of USP25 seen in our experimental platform are not owing to the modulation of IL17. We also are intrigued by the underlying mechanisms and why *Usp25*$^{-/-}$ has no effect on IL17-induced inflammatory factors. First, it is possible that IL17 produced through NF-κB activation may show proinflammatory effects at a later time point. There are recent studies that have shown that IL17 modulates macrophage phenotype in a NF-κB–dependent manner after 48 hours of exposure.[49] Other studies, using a similar condition media experimental design, have shown that inflammatory factors may be induced by IL17 in macrophages after 24 hours.[50] Second, inflammatory factor induced by IL17, which may be independent of USP25, also may involve noncanonical factors such as glycogen synthase kinase 3 and CCAAT enhancer binding protein alpha. Therefore, a comprehensive study is needed to elucidate the possible mechanisms in the future.

One puzzling finding in our study is related to STING. STING is an important protein that regulates the transcription of host defense genes such as type I IFNs and proinflammatory cytokines. STING forms a complex with TBK1, and this complex phosphorylates IRF3 and NF-κB. Our studies showed that L-arginine–induced AP increases the

expression of STING, indicating that at least some NF-κB activation may be attributed to STING up-regulation. However, *Usp25*$^{-/-}$ mice do not show this increase in STING but still up-regulate TBK1/NF-κB. This raises the question of how USP25 may induce TBK1 phosphorylation and activation. Previous studies have shown that TBK1 stability could be regulated by ubiquitinating modification.[51] It has been reported further that USP19 promotes TBK1 degradation through chaperone-mediated autophagy.[52] Severe acute respiratory syndrome coronavirus 2 M protein also interacts with TBK1 and induces TBK1 degradation by K48-linked ubiquitination.[53] However, *Usp25* deficiency in our study increased TBK1 phosphorylation but failed to change the TBK1 protein levels, indicating that USP25 does not affect TBK1 protein stability or deubiquitination. Empirically, we found no direct association between USP25 and TBK1 using lysates from macrophages or pancreatic tissue from WT mice (data not shown).

Conclusions

Our study shows a novel role of macrophage-expressed USP25 in AP. Deficiency in macrophage USP25 enhances the activation of the TBK1/NF-κB pathway, resulting in elaboration of cytokines and type I interferon-related genes. *Usp25* deficiency exacerbated pancreatic and lung injury induced by L-arginine, cerulein, and CDE, and increased neutrophil and macrophage infiltration and systemic inflammatory responses. Thus, approaches to increase USP25 expression and function in macrophages may provide an anti-inflammatory therapy for AP.

Methods

Animal Experiments

All animal studies were approved by the Institutional Animal Policy and Welfare Committee of Wenzhou Medical University (approval: wydw2021-142). C57BL/6 mice were obtained from Gempharmatech, Co, Ltd (Nanjing, China). USP25$^{-/-}$ mice on a C57BL/6 background were provided by Professor Jian Yuan (Tongji University, Shanghai, China). All mice were housed under specific-pathogen free conditions with 50% $\pm$ 5% humidity at 22°C $\pm$ 2.0°C and under a 12/12-hour light/dark cycle. Mice were fed a standard chow diet (CD). We generated 3 models of AP in WT and *Usp25*$^{-/-}$ mice: L-arginine, cerulein, and CDE.

L-arginine–induced pancreatitis. Male mice at 8 weeks of age were fasted for 14 hours. Pancreatitis was induced by 2 intraperitoneal injections of L-arginine at a dose of 4 g/kg (A5131; Sigma) at 1-hour intervals.[54] Control mice received the same volume of saline by intraperitoneal injections. Mice were killed 72 hours after the first injection. Serum, pancreas, and lung samples were collected for analyses. Pancreas-weight-to-body-weight ratios were recorded to assess edema.

Cerulein-induced pancreatitis. Male mice at 8 weeks of age were fasted for 14 hours, and then pancreatitis was induced by 8 intraperitoneal injections of cerulein administered at a dose of 50 μg/kg at a 1-hour interval.[55] Control mice received saline at the same time. Mice were killed 21 hours after the first injection. Serum, pancreas, and lung samples were collected.

CDE model of pancreatitis. Female mice at 4 weeks of age were fasted for 12 hours. Mice then were fed a choline-deficient diet (XTCD10; Xietong, Jiangsu, China) supplemented with 0.5% dextroisomer and Levoisomer-ethionine (E117217; Aladdin, Shanghai, China) for 3 days.[12] Control mice were fed a standard rodent chow diet (CD). Tissues were harvested at the experimental end point. For some studies, we examined the survival of mice after CDE feeding. Mice were fasted for 12 hours and fed a CDE for 4 days, followed by a normal diet for another 4 days.

To examine the role of NF-κB in AP models, male *Usp25*$^{-/-}$ mice at 8 weeks of age were fasted for 14 hours. Mice then were administered NF-κB inhibitor at 5 or 10 mg/kg BAY 11-7082 (HY-13453; Medchem Express, Monmouth Junction, NJ) by intragastric infusion. Six hours later, mice received 2 intraperitoneal injections of L-arginine at a dose of 4 g/kg at 1-hour intervals. Mice received 5 or 10 mg/kg BAY 11-7082 again 6 hours after the last L-arginine injection. Tissues were harvested at 72 hours from the first L-arginine injection.

Blood samples from mice were used to prepare serum. Samples then were subjected to amylase activity and lipase activity tests using commercially available assay kits (BioAssay Systems, Hayward, CA). A lactate dehydrogenase kit (BioAssay Systems) was used to measure the LDH activity. In addition, IFNβ levels in mouse serum were determined using enzyme-linked immunosorbent assay (ELISA) kits (R&D Systems, Minneapolis, MN).

Bone Marrow Transplantation

Bone marrow chimeric mice were generated as previously described.[9] WT recipient mice were subjected to irradiation with a dose of 6 Gy. Bone marrow cells isolated from the femur and tibia of either WT or *Usp25*$^{-/-}$ mice were administered in donors at 5.0 $\times$ 10^6 by tail vein injection. Eight weeks later, WT$\rightarrow$WT and KO$\rightarrow$WT mice were subjected to AP modeling using the L-arginine method described earlier.

Isolation of BMDMs

BMDMs were isolated from the femur and tibia of WT and *Usp25*$^{-/-}$ mice. Briefly, bones were flushed with RPMI 1640 containing 100 U/mL penicillin and 100 μg/mL streptomycin. Then, samples were filtered using a 70-mm nylon mesh and collected in 50-mL tubes. Red blood cell lysis was performed (R1010; Solarbio, Beijing, China) and samples were spun at 1000 $\times$ *g* for 5 minutes. Cells were cultured in 20% L929 cell culture medium. On days 3 and 5, fresh Dulbecco's modified Eagle medium (DMEM) containing 20% L929 cell culture medium and 10% fetal bovine serum was added. Cells were used for experiments on day 7. Studies included exposure of BMDMs to the following: acinar cell supernatant to assess activation, STING agonist DMXAA for signaling pathway determination, and IL17A to assess crosstalk between signaling axes. After exposure of

BMDMs to acinar cell supernatant, levels of IFNβ were detected by ELISA.

For some studies, BMDMs isolated from Usp25$^{-/-}$ mice were transfected with control (B21030500; Genechem, Shanghai, China) or plasmid expressing Flag-tagged *Usp25* (NM_013918; Genechem).

Isolation of Pancreatic Acinar Cells

Pancreatic acinar cells were isolated from 8- to 10-week-old WT and *Usp25*$^{-/-}$ mice by a collagenase digestion method, essentially as previously described.[56] Briefly, pancreas tissue was cut into 1-mm^3 pieces and digested in DMEM supplemented with 1 mg/mL collagenase type 4 (LS004188; Worthington, Lakewood, NJ), 2.5 mg/mL bovine serum albumin (BSA) (A1933; Sigma), and 100 μg/mL soybean trypsin inhibitor (SBTI) (LS003571; Worthington) at 37°C for 20 minutes. The digestion was repeated once more with fresh media. Digested sample was passed through a 100-μm nylon mesh and rinsed with DMEM containing 10 mg/mL BSA and 100 μg/mL SBTI. Cells were gently layered onto culture plates using a transfer pipette. Once cells had settled, the supernatant was replaced with fresh DMEM supplemented with 40 mg/mL BSA and 100 μg/mL SBTI. Cells were centrifuged at 50 $\times$ *g* and resuspended in the same formulation. After 2 more washes, cells were resuspended in DMEM supplemented with 1 mg/mL BSA and 100 μg/mL SBTI and cultured. After 30 minutes, supernatant was collected (time zero) and used to expose BMDMs. A 24-hour supernatant also was collected and tested on BMDMs. A lactate dehydrogenase assay was performed on 0- and 24-hour supernatant samples. Cells also were examined for cell death by trypan blue exclusion test.

MPO Assay

MPO activity was measured in pancreatic and lung lysates using methods described previously.[57,58] Tissues were homogenized in 0.1 mol/L phosphate buffer (pH 7.4) containing protease inhibitors (P1051; Beyotime, Shanghai, China) with Tissuelyser (Jingxin, Shanghai, China). Samples were centrifuged at 16,000 $\times$ *g* for 15 minutes at 4°C. The pellets were resuspended in 0.1 mol/L phosphate buffer (pH 5.4) containing 0.5% hexadecyltrimethylammonium bromide (H6269; Sigma), 10 mmol/L ethylene diamine tetra-acetic acid, and protease inhibitors. The pellets further were subjected to 3 cycles of sonification, freezing, and thawing. The extract then was centrifuged, and the supernatant was used for MPO assay. MPO levels were measured by a colorimetry method using 3,3′,5,5′-tetramethylbenzidine with 0.03% H_2O_2. The reaction was stopped with 2 N H_2SO_4. Optical density was read at 450 nm. The protein concentration of the supernatant were measured using the Micro BCA Protein Assay Kit (23235; Thermo, Carlsbad, CA). MPO protein (M6908; Sigma) was used to establish the standard curve. MPO levels were expressed in mU/mg protein.

Histology and Immunohistochemistry

Pancreas and lung tissues were fixed in 4% paraformaldehyde and embedded in paraffin. Slices at 5-μm were prepared. Slides were dewaxed and rehydrated. For histopathologic assessment, slides were stained with H&E. Injury scores were graded from 0 to 3 as described.[59,60] Briefly, scores were generated for edema (0, absent; 1, diffuse expansion of interlobar; 2, same as 1 + diffuse expansion of interacinar; and 3, same as 2 + diffuse expansion of intercellular), inflammatory infiltration (0, absent; 1, around pancreatic duct; 2, intralobular or perivascular, <50% of the lobules; and 3, intralobular or perivascular, >50% of the lobules), and necrosis (0, absent; 1, periductal necrosis, <10% of cells; 2, focal acinar cells necrosis, 30%–50% of cells; and 3, diffuse acinar cells necrosis, >50% of cells).

For immunohistochemistry, dewaxed and rehydrated sections were subjected to antigen retrieval in 0.01 mol/L citrate buffer (pH 6.0) for 3 minutes at boiling temperatures. Slides then were blocked with 3% H_2O_2 for 30 minutes at

Table 1. Reverse-Transcription Quantitative Polymerase Chain Reaction Primer Sequences for Mouse Genes

Gene	Forward primer	Reverse primer
Ccl4	TTCCTGCTGTTTCTCTTACACCT	CTGTCTGCCTCTTTTGGTCAG
Ccl5	GCTGCTTTGCCTACCTCTCC	TCGAGTGACAAACACGACTGC
Cxcl10	AAGTGCTGCCGTCATTTTCTG	TTCCCTATGGCCCTCATTCTC
Isg15	GGTGTCCGTGACTAACTCCAT	TGGAAAGGGTAAGACCGTCCT
Ifnb	CAGCTCCAAGAAAGGACGAAC	GGCAGTGTAACTCTTCTGCAT
Il17a	TTTAACTCCCTTGGCGCAAAA	CTTTCCCTCCGCATTGACAC
Tnf	CTGAGGTCAATCTGCCCAAGTAC	CTTCACAGAGCAATGACTCCAAAG
Cxcl1	CACCCAAACCGAAGTCATAGC	TTGGGGACACCTTTTAGCATCT
Cxcl5	TGCGTTGTGTTTGCTTAACCG	CTTCCACCGTAGGGCACTG
Ccl7	GCTGCTTTCAGCATCCAAGTGC	CCAGGGACACCGACTACTG
Ccl20	GCCTCTCGTACATACAGACGC	CCAGTTCTGCTTTGGATCAGC
*Rna18s**	AGTCCCTGCCCTTTGTACACA	CGATCCGAGGGCCTCACT

**Rna18s* was used as the housekeeping gene. Data were normalized by ΔΔ cyle threshold method.

room temperature. Primary antibodies against macrophage antigen F4/80 (1:400) and MPO (1:25) were applied for 2 hours at room temperature. Horseradish peroxidase–linked secondary antibodies and diaminobenzidine (brown color) were used for detection. Images were taken using bright-field illumination on an epifluorescence microscope equipped with digital camera (Nikon, Tokyo, Japan).

Pancreatic Trypsin Activity Assay

Pancreatic tissue was homogenized in ice-cold buffer containing 5 mmol/L 4-morpholineethanesulfonic acid (pH 6.5), 1 mmol/L $MgSO_4$, and 250 mmol/L sucrose. Samples then were mixed with assay buffer containing 50 mmol/L Tris-HCl (pH = 8.0), 150 mmol/L NaCl, 1 mmol/L $CaCl_2$, and 0.1 mg/mL BSA. Trypsin activity was determined by adding Boc-GIn-Ala-Arg-MCA·HCl[61] (4017019; Bachem, Bubendorf, Switzerland). Excitation/emission at 380 nm/440 nm was measured.[62,63] Purified trypsin (Worthington) was used to generate a standard curve.

RNA Isolation and Quantitative Real-Time Polymerase Chain Reaction

Total RNA was isolated from mouse tissues and cultured BMDMs using TRIzol (Thermo Fisher, Carlsbad, CA). A total of 1 μg RNA was used for reverse-transcription with PrimeScript reverse transcription reagent with genomic DNA Eraser (Takara, Beijing, China). Quantitative polymerase chain reaction was conducted using TB Green Premix Ex Taq II (Takara) and the CFX96 Real-Time System (Bio-Rad, Hercules, CA). Primer sequences are listed in Table 1.

Immunoblotting Assay

Lysates were prepared from cultured BMDMs and mouse tissues in RIPA buffer (P0013B; Beyotime) containing protease and phosphatase inhibitor cocktail (P1051; Beyotime). Protein concentrations were measured using a quick start Bradford kit (Bio-Rad). Approximately 40 μg total proteins were loaded and electrophoresed in 10% sodium dodecyl sulfate–polyacrylamide gels. Samples then were transferred to polyvinylidene difluoride membranes (Bio-Rad). Membranes were blocked with 5% skim milk for 1 hour, and then incubated overnight with primary antibodies. Horseradish-conjugated secondary antibodies and enhanced chemiluminescence substrates were used for detection with the ChemiDoc XRS$^+$ system (Bio-Rad). ImageJ analysis software version 1.38e (National Institutes of Health, Bethesda, MD) was used for densitometric quantification of blots.

Antibodies against STING (13647), phosphorylated (p)-TBK1 (Ser172; 5483), TBK1 (3013), p–IRF-3 (Ser396; 4947), IRF-3 (4302), p–NF-κB p65 (Ser536; 3033), NF-κB p65 (8242), NF-kappa-B inhibitor alpha (4812), p-stress-activated protein kinase/JNK (Thr183/Tyr185; 4668), SAPK/JNK (9252), p-Erk1/2 (Thr202/Tyr204; 4370), Erk1/2 (4695), p-p38 (Thr180/Tyr182; 9211), p38 (8690), and glyceraldehyde-3-phosphate dehydrogenase (5174) were obtained from Cell Signaling Technology (Pudong, Shanghai, China). Antibodies against TRAF6 (66498-1–Ig), TRAF3 (18099-1–AP), and FLAG Tag (20543-1–AP) were obtained from Peprotech (Cranbury, NJ). TLR4 (sc-293072) antibody was obtained Santa Cruz, CA, and USP25 (ab187156) was from Abcam (Cambridge, MA).

Enzyme-Linked Immunosorbent Assay

IFNβ levels in sera and acini cell culture supernatant were determined with an ELISA kit according the manufacturer's protocol (R&D Systems).

Statistical Analysis

All data are expressed as means ± SD. Statistical analyses were performed using GraphPad Pro Prism 8.0 (GraphPad, San Diego, CA). The Student t test or 1-way analysis of variance followed by the multiple comparisons test with Bonferroni correction was used to analyze the differences between sets of data. A P value less than .05 was considered significant.

References

1. Petrov MS, Yadav D. Global epidemiology and holistic prevention of pancreatitis. Nat Rev Gastroenterol Hepatol 2019;16:175–184.
2. Volzke H, Baumeister SE, Alte D, Hoffmann W, Schwahn C, Simon P, John U, Lerch MM. Independent risk factors for gallstone formation in a region with high cholelithiasis prevalence. Digestion 2005;71:97–105.
3. Gukovskaya AS, Pandol SJ, Gukovsky I. New insights into the pathways initiating and driving pancreatitis. Curr Opin Gastroenterol 2016;32:429–435.
4. Yadav D, Whitcomb DC. The role of alcohol and smoking in pancreatitis. Nat Rev Gastroenterol Hepatol 2010;7:131–145.
5. Boxhoorn L, Voermans RP, Bouwense SA, Bruno MJ, Verdonk RC, Boermeester MA, van Santvoort HC, Besselink MG. Acute pancreatitis. Lancet 2020;396:726–734.
6. Schepers NJ, Bakker OJ, Besselink MG, Ali UA, Bollen TL, Gooszen HG, van Santvoort HC, Bruno MJ, Dutch Pancreatitis Study Group. Impact of characteristics of organ failure and infected necrosis on mortality in necrotising pancreatitis. Gut 2019;68:1044–1051.
7. Lee PJ, Papachristou GL. New insights into acute pancreatitis. Nat Rev Gastroenterol Hepatol 2019;16:479–496.
8. Crockett SD, Wani S, Gardner TB, Falck-Ytter Y, Barkun AN, American Gastroenterological Association Institute. American Gastroenterological Association Institute guideline on initial management of acute pancreatitis. Gastroenterology 2018;154:1096–1101.
9. Chen TW, Huang WJ, Qian JF, Luo W, Shan PR, Cai Y, Lin K, Wu GJ, Liang G. Macrophage-derived myeloid differentiation protein 2 plays an essential role in ox-LDL-induced inflammation and atherosclerosis. EBioMedicine 2020;53:102706.
10. Sendler M, Weiss F-U, Golchert J, Homuth G, van den Brandt C, Mahajan UM, Partecke L-I, Doering P, Gukovsky I, Gukovskaya AS, Wagh PR, Lerch MM,

Mayerle J. Cathepsin B-mediated activation of trypsinogen in endocytosing macrophages increases severity of pancreatitis in mice. Gastroenterology 2018;154:704.
11. Jakkampudi A, Jangala R, Reddy BR, Mitnala S, Reddy DN, Talukdar R. NF-kappa B in acute pancreatitis: mechanisms and therapeutic potential. Pancreatology 2016;16:477–488.
12. Watanabe T, Kudo M, Strober W. Immunopathogenesis of pancreatitis. Mucosal Immunol 2017;10:283–298.
13. Zhao QL, Wei Y, Pandol SJ, Li LY, Habtezion A. STING Signaling promotes inflammation in experimental acute pancreatitis. Gastroenterology 2018;154:1822.
14. Ge P, Luo YL, Okoye CS, Chen HY, Liu JY, Zhang GX, Xu CM, Chen HL. Intestinal barrier damage, systemic inflammatory response syndrome, and acute lung injury: a troublesome trio for acute pancreatitis. Biomed Pharmacother 2020;132:110770.
15. Mayer J, Rau B, Gansauge F, Beger HG. Inflammatory mediators in human acute pancreatitis: clinical and pathophysiological implications. Gut 2000;47:546–552.
16. Habtezion A. Inflammation in acute and chronic pancreatitis. Curr Opin Gastroenterol 2015;31:395–399.
17. Montecucco F, Mach F, Lenglet S, Vonlaufen A, Gomes Quindere AL, Pelli G, Burger F, Galan K, Dallegri F, Carbone F, Proudfoot AE, Vuilleumier N, Frossard JL. Treatment with Evasin-3 abrogates neutrophil-mediated inflammation in mouse acute pancreatitis. Eur J Clin Invest 2014;44:940–950.
18. Folias AE, Penaranda C, Su AL, Bluestone JA, Hebrok M. Aberrant innate immune activation following tissue injury impairs pancreatic regeneration. PLoS One 2014;9:e102125.
19. Valero R, Marfany G, Gonzalez-Angulo O, Gonzalez-Gonzalez G, Puelles L, Gonzalez-Duarte R. USP25, a novel gene encoding a deubiquitinating enzyme, is located in the gene-poor region 21q11.2. Genomics 1999;62:395–405.
20. Zhu WJ, Zheng DD, Wang DD, Yang LH, Zhao CG, Huang XY. Emerging roles of ubiquitin-specific protease 25 in diseases. Front Cell Dev Biol 2021;9:698751.
21. Ding C, Li F, Long Y, Zheng J. Chloroquine attenuates lipopolysaccharide-induced inflammatory responses through upregulation of USP25. Can J Physiol Pharmacol 2017;95:481–491.
22. Zhong B, Liu X, Wang X, Chang SH, Liu X, Wang A, Reynolds JM, Dong C. Negative regulation of IL-17-mediated signaling and inflammation by the ubiquitin-specific protease USP25. Nat Immunol 2012;13:1110–1117.
23. Zhong B, Liu X, Wang X, Liu X, Li H, Darnay BG, Lin X, Sun S-C, Dong C. Ubiquitin-specific protease 25 regulates TLR4-dependent innate immune responses through deubiquitination of the adaptor protein TRAF3. Sci Signal 2013;6:ra35.
24. Zhong HJ, Wang D, Fang LR, Zhang H, Luo R, Shang M, Ouyang C, Ouyang HP, Chen HC, Xiao SB. Ubiquitin-specific proteases 25 negatively regulates virus-induced type i interferon signaling. PLoS One 2013;8:e80976.
25. Dawra R, Sharif R, Phillips P, Dudeja V, Dhaulakhandi D, Saluja AK. Development of a new mouse model of acute pancreatitis induced by administration of L-arginine. Am J Physiol Gastrointest Liver Physiol 2007;292:G1009–G1018.
26. Hu F, Lou N, Jiao J, Guo F, Xiang H, Shang D. Macrophages in pancreatitis: mechanisms and therapeutic potential. Biomed Pharmacother 2020;131:110693.
27. Wang J, Ohmuraya M, Suyama K, Hirota M, Ozaki N, Baba H, Nakagata N, Araki K, Yamamura K. Relationship of strain-dependent susceptibility to experimentally induced acute pancreatitis with regulation of Prss1 and Spink3 expression. Lab Invest 2010;90:654–664.
28. Lombardi B, Estes LW, Longnecker DS. Acute hemorrhagic pancreatitis (massive necrosis) with fat necrosis induced in mice by DL-ethionine fed with a choline-deficient diet. Am J Pathol 1975;79:465–480.
29. Lin D, Zhang M, Zhang MX, Ren Y, Jin J, Zhao Q, Pan Z, Wu M, Shu HB, Dong C, Zhong B. Induction of USP25 by viral infection promotes innate antiviral responses by mediating the stabilization of TRAF3 and TRAF6. Proc Natl Acad Sci U S A 2015;112:11324–11329.
30. Li J, Tan Q, Yan M, Liu L, Lin H, Zhao F, Bao G, Kong H, Ge C, Zhang F, Yu T, Li J, He X, Yao M. miRNA-200c inhibits invasion and metastasis of human non-small cell lung cancer by directly targeting ubiquitin specific peptidase 25. Mol Cancer 2014;13:166.
31. Wang X-M, Yang C, Zhao Y, Xu Z-G, Yang W, Wang P, Lin D, Xiong B, Fang J-Y, Dong C, Zhong B. The deubiquitinase USP25 supports colonic inflammation and bacterial infection and promotes colorectal cancer. Nat Cancer 2020;1:811–825.
32. Xu DC, Liu JP, Fu T, Shan B, Qian LH, Pan LF, Yuan JY. USP25 regulates Wnt signaling by controlling the stability of tankyrases. Genes Dev 2017;31:1024–1035.
33. Li G, Chen H, Liu L, Xiao P, Xie Y, Geng X, Zhang T, Zhang Y, Lu T, Tan H, Li L, Sun B. Role of interleukin-17 in acute pancreatitis. Front Immunol 2021;12:674803.
34. Thomson JE, Brand M, Fonteh P. The immune imbalance in the second hit of pancreatitis is independent of IL-17A. Pancreatology 2018;18:246–252.
35. Peng C, Li ZQ, Yu X. The role of pancreatic infiltrating innate immune cells in acute pancreatitis. Int J Med Sci 2021;18:534–545.
36. Gukovskaya AS, Gukovsky I, Alguel H, Habtezion A. Autophagy, inflammation, and immune dysfunction in the pathogenesis of pancreatitis. Gastroenterology 2017;153:1212–1226.
37. Jakkampudi A, Jangala R, Reddy R, Mitnala S, Rao GV, Pradeep R, Reddy DN, Talukdar R. Acinar injury and early cytokine response in human acute biliary pancreatitis. Sci Rep 2017;7:15276.
38. Wan JH, Ren YP, Yang XY, Li XY, Xia L, Lu NH. The role of neutrophils and neutrophil extracellular traps in acute pancreatitis. Front Cell Dev Biol 2021;8:565758.
39. Tokoro T, Makino I, Harada S, Okamoto K, Nakanuma S, Sakai S, Kinoshita J, Nakamura K, Miyashita T, Tajima H, Ninomiya I, Fushida S, Ohta T. Interactions between neutrophils and platelets in the progression of acute pancreatitis. Pancreas 2020;49:830–836.
40. Merza M, Hartman H, Rahman M, Hwaiz R, Zhang E, Renstrom E, Luo L, Morgelin M, Regner S, Thorlacius H. Neutrophil extracellular traps induce trypsin activation,

inflammation, and tissue damage in mice with severe acute pancreatitis. Gastroenterology 2015;149:1920.
41. Huang Q, Cheng X, Luo C, Yang S, Li S, Wang B, Yuan X, Yang Y, Wen Y, Liu R, Tang L, Sun H. Placental chorionic plate-derived mesenchymal stem cells ameliorate severe acute pancreatitis by regulating macrophage polarization via secreting TSG-6. Stem Cell Res Ther 2021;12:337.
42. Wu JH, Zhang L, Shi JJ, He RZ, Yang WJ, Habtezion A, Niu NN, Lu P, Xue J. Macrophage phenotypic switch orchestrates the inflammation and repair/regeneration following acute pancreatitis injury. EBioMedicine 2020; 58:12.
43. Liu J, Niu ZQ, Zhang R, Peng Z, Wang LM, Liu Z, Gao YX, Pei HH, Pan LF. MALAT1 shuttled by extracellular vesicles promotes M1 polarization of macrophages to induce acute pancreatitis via miR-181a-5p/HMGB1 axis. J Cell Mol Med 2021;25:9241–9254.
44. Hoque R, Sohail M, Malik A, Sarwar S, Luo Y, Shah A, Barrat F, Flavell R, Gorelick F, Husain S, Mehal W. TLR9 and the NLRP3 inflammasome link acinar cell death with inflammation in acute pancreatitis. Gastroenterology 2011;141:358–369.
45. Sendler M, van den Brandt C, Glaubitz J, Wilden A, Golchert J, Weiss FU, Homuth G, Chama LLD, Mishra N, Mahajan UM, Bossaller L, Volker U, Broker BM, Mayerle J, Lerch MM. NLRP3 inflammasome regulates development of systemic inflammatory response and compensatory anti-inflammatory response syndromes in mice with acute pancreatitis. Gastroenterology 2020;158:253.
46. Li XY, He C, Li NS, Ding L, Chen HY, Wan JH, Yang XY, Xia L, He WH, Xiong HF, Shu X, Zhu Y, Lu NH. The interplay between the gut microbiota and NLRP3 activation affects the severity of acute pancreatitis in mice. Gut Microbes 2020;11:1774–1789.
47. Saeki K, Kanai T, Nakano M, Nakamura Y, Miyata N, Sujino T, Yamagishi Y, Ebinuma H, Takaishi H, Ono Y, Takeda K, Hozawa S, Yoshimura A, Hibi T. CCL2-induced migration and SOCS3-mediated activation of macrophages are involved in cerulein-induced pancreatitis in mice. Gastroenterology 2012;142:1010-U526.
48. Manohar M, Jones EK, Rubin SJS, Subrahmanyam PB, Swaminathan G, Mikhail D, Bai L, Singh G, Wei Y, Sharma V, Siebert JC, Maecker HT, Husain SZ, Park WG, Pandol SJ, Habtezion A. Novel circulating and tissue monocytes as well as macrophages in pancreatitis and recovery. Gastroenterology 2021;161:2014–2029.e14.
49. Wen J, Bai H, Chen N, Zhang WF, Zhu XW, Li PZ, Gong JP. USP25 promotes endotoxin tolerance via suppressing K48-linked ubiquitination and degradation of TRAF3 in Kupffer cells. Mol Immunol 2019;106:53–62.
50. Shen J, Sun X, Pan B, Cao S, Cao J, Che D, Liu F, Zhang S, Yu Y. IL-17 induces macrophages to M2-like phenotype via NF-kappaB. Cancer Manag Res 2018;10:4217–4228.
51. Yuan C, Yang D, Ma J, Yang J, Xue J, Song F, Liu X. Modulation of Wnt/beta-catenin signaling in IL-17A-mediated macrophage polarization of RAW264.7 cells. Braz J Med Biol Res 2020;53:e9488.
52. Meng ZY, Xu R, Xie LX, Wu YT, He Q, Gao P, He XH, Chen Q, Xie Q, Zhang JQ, Yang QW. A20/Nrdp1 interaction alters the inflammatory signaling profile by mediating K48-and K63-linked polyubiquitination of effectors MyD88 and TBK1. J Biol Chem 2021;297:100811.
53. Zhao H, Wang W, Zhang J, Liang T, Fan GP, Wang ZW, Zhang PD, Wang X, Zhang J. Inhibition of osteopontin reduce the cardiac myofibrosis in dilated cardiomyopathy via focal adhesion kinase mediated signaling pathway. Am J Transl Res 2016;8:3645–3655.
54. Sui LY, Zhao YH, Wang WF, Wu P, Wang ZD, Yu Y, Hou ZJ, Tan GY, Liu Q. SARS-CoV-2 membrane protein inhibits type I interferon production through ubiquitin-mediated degradation of TBK1. Front Immunol 2021;12:662989.
55. Park MJ, Iyer S, Xue X, Cunha JB, Gu SF, Moons D, Pipe SW, Williams JA, Simeone DM, Shah YM, Omary MB. HIF1-alpha regulates acinar cell function and response to injury in mouse pancreas. Gastroenterology 2018;154:1630.
56. Jancso Z, Sahin-Toth M. Mutation that promotes activation of trypsinogen increases severity of secretagogue-induced pancreatitis in mice. Gastroenterology 2020;158:1083–1094.
57. Dawra R, Ku YS, Sharif R, Dhaulakhandi D, Phillips P, Dudeja V, Saluja AK. An improved method for extracting myeloperoxidase and determining its activity in the pancreas and lungs during pancreatitis. Pancreas 2008; 37:62–68.
58. Romac JMJ, Shahid RA, Swain SM, Vigna SR, Liddle RA. Piezo1 is a mechanically activated ion channel and mediates pressure induced pancreatitis. Nat Commun 2018;9:1715.
59. Wildi S, Kleeff J, Mayerle J, Zimmermann A, Bottinger EP, Wakefield L, Buchler MW, Friess H, Korc M. Suppression of transforming growth factor beta signalling aborts caerulein induced pancreatitis and eliminates restricted stimulation at high caerulein concentrations. Gut 2007;56:685–692.
60. Hernandez G, Luo T, Javed TA, Wen L, Kalwat MA, Vale K, Ammouri F, Husain SZ, Kliewer SA, Mangelsdorf DJ. Pancreatitis is an FGF21-deficient state that is corrected by replacement therapy. Sci Transl Med 2020;12:eaay5186.
61. Kawabata S, Miura T, Morita T, Kato H, Fujikawa K, Iwanaga S, Takada K, Kimura T, Sakakibara S. Highly sensitive peptide-4-methylcoumaryl-7-amide substrates for blood-clotting proteases and trypsin. Eur J Biochem 1988;172:17–25.
62. Gukovskaya AS, Vaquero E, Zaninovic V, Gorelick FS, Lusis AJ, Brennan ML, Holland S, Pandol SJ. Neutrophils and NADPH oxidase mediate intrapancreatic trypsin activation in murine experimental acute pancreatitis. Gastroenterology 2002;122:974–984.
63. Gukovsky I, Cheng JH, Nam KJ, Lee OT, Lugea A, Fischer L, Penninger JM, Pandol SJ, Gukovskaya AS. Phosphatidylinositide 3-kinase gamma regulates key pathologic responses to cholecystokinin in pancreatic acinar cells. Gastroenterology 2004;126:554–566.

Received November 17, 2021. Accepted July 18, 2022.

Correspondence
Address correspondence to: Yi Wang, PhD, Chemical Biology Research Center, School of Pharmaceutical Sciences, Wenzhou Medical University, Wenzhou, Zhejiang 325035, China. e-mail: yi.wang1122@wmu.edu.cn; fax: (86) 577 85773060

Acknowledgments

The authors thank Professor Jian Yuan (Fudan University, Shanghai, China) for providing *Usp25*$^{-/-}$ mice. The authors also thank Professor Zia Ali Khan (Western University of Ontario, London, Canada) for language editing of the manuscript.

CRediT Authorship Contributions

Xin Liu (Data curation: Equal; Formal analysis: Lead; Investigation: Lead; Writing – original draft: Equal; Writing – review & editing: Equal)

Wu Luo (Formal analysis: Equal; Funding acquisition: Supporting; Investigation: Equal; Methodology: Supporting)

Jiahao Chen (Investigation: Supporting)

Chenghong Hu (Investigation: Supporting)

Rumbidzai N. Mutsinze (Investigation: Supporting)

Xu Wang (Formal analysis: Supporting)

Yanmei Zhang (Investigation: Supporting)

Lijiang Huang (Conceptualization: Supporting; Writing – review & editing: Supporting)

Wei Zuo (Conceptualization: Supporting; Writing – review & editing: Supporting)

Guang Liang (Conceptualization: Equal; Formal analysis: Equal; Funding acquisition: Equal; Investigation: Equal; Writing – original draft: Equal)

Yi Wang (Conceptualization: Equal; Data curation: Equal; Formal analysis: Equal; Funding acquisition: Lead; Supervision: Lead; Writing – original draft: Equal; Writing – review & editing: Lead)

Conflicts of interest

The authors disclose no conflicts.

Funding

This study was supported by National Key Research Project grant 2017YFA0506000 (Y.W.); National Natural Science Foundation of China grants 21961142009 (G.L.), 82000793 (W.L.), and 82170373 (Y.W.); Zhejiang Provincial Key Scientific Project grant 2021C03041 (G.L.); and Natural Science Foundation of Zhejiang Province grant LR18H160003 (Y.W.).